



RESEARCH ARTICLE

10.1002/2015JD024129

Key Points:

- Examination of the spatiotemporal variation of I_p across land/water boundaries
- Evaluating hypotheses for explaining the variation
- Variations are not likely related to range of detection, cloud top height, or CG activity

Correspondence to:

T. Chronis,
themis.chronis@nsstc.uah.edu

Citation:

Chronis, T., W. Koshak, and E. McCaul (2016), Why do oceanic negative cloud-to-ground lightning exhibit larger peak current values?, *J. Geophys. Res. Atmos.*, 121, 4049–4068, doi:10.1002/2015JD024129.

Received 25 AUG 2015

Accepted 29 MAR 2016

Accepted article online 6 APR 2016

Published online 22 APR 2016

Why do oceanic negative cloud-to-ground lightning exhibit larger peak current values?

T. Chronis¹, W. Koshak², and E. McCaul³

¹Earth System Science Center, University of Alabama in Huntsville, Huntsville, Alabama, USA, ²Earth Science Office, ZP11, NASA Marshall Space Flight Center, Huntsville, Alabama, USA, ³Universities Space Research Association, Huntsville, Alabama, USA

Abstract This study examines the temporal (monthly) and spatial climatology (2004–2010) of the first return stroke of the cloud-to-ground (CG) lightning flash peak current (I_p) across various land/water boundaries over the contiguous United States. Four regions are examined: the Gulf of Mexico (region 1), the Florida peninsula (region 2), Lake Michigan (region 3), and part of the U.S. Mid-Atlantic (region 4). The cross sections across the coastlines of regions 1, 2, and 4 show a gradual oceanward increase in the mean negative polarity CG peak current values ($-I_p$). This transition along the respective land/ocean boundaries is not sharp but gradual. In direct contrast with ocean, there is no consistent behavior in $-I_p$ values as we move from land out across the fresh water of Lake Michigan (region 3). Meanwhile, the positive CG flash peak current ($+I_p$) values do not exhibit a consistent variation across any coastal boundary. For region 1, the $-I_p$ values increase as we move toward the coast (southwards) especially during the wet season (June–October). This finding is in direct contrast with studies that documented winter as the season of maximum $-I_p$ values. The zonal and seasonal variations of $-I_p$ values across region 4 are not quite as pronounced, but the oceanic $-I_p$ values are still larger than over the adjoining landmass. We explore in turn which up to date hypotheses pertinent to the oceanic $-I_p$ enhancement are supported or refuted by our findings. It is concluded that the oceanic $-I_p$ enhancement is not an artifact related to CG detection or I_p retrieval methods, nor is it likely related to the cloud top heights or CG activity. The study cannot refute the role of electrical conductivity and its contribution to CG leader attachment processes. However, given the observed “blurred transition” of the I_p values across the coastlines this paper suggests that likely the main physical mechanism is acting on the thundercloud potential. The recently suggested role of sodium chloride (NaCl) but also the role of ice crystal size (implicated herein), as possible modulators of the thundercloud potential, exhibit distinct pros and cons. Their candidacy is supported by their strong physical links to the electrostatic charging and thundercloud electric potential buildup but also by the exhibited blurred $-I_p$ transition across the coastlines. In contrast, the suggested mechanisms cannot individually explain the observed $-I_p$ enhancement in terms of season, NaCl concentrations, and absence of similar behavior in the respective $+I_p$ values.

1. Introduction

The differences between oceanic and continental lightning flash properties have been the focal point for studies that appeared during the late 1970s [Turman, 1977; Toland and Vonnegut, 1977]. Ground-based [e.g., see Lyons *et al.*, 1998a; Hutchins *et al.*, 2013] and space-based observations [e.g., see Mach *et al.*, 2011; Beirle *et al.*, 2014] indicate that lightning flash energetic proxies exhibit larger values over the oceans than over land. In recent years, the advancements in ground-based lightning locating systems have provided information beyond the lightning flash timing and location. Studies by Lyons *et al.* [1998a], Huffines and Orville [1999], Orville and Huffines [2001], and others have convincingly documented larger values for the oceanic negative cloud-to-ground (CG) first return stroke peak current (I_p), but these observations are exclusively related to the negative polarity CG (−CG) [Cummins *et al.*, 2005; Orville *et al.*, 2011; Cooray *et al.*, 2014]. This finding has received additional support from regional observations worldwide [Füllekrug *et al.*, 2002; Rivas Soriano *et al.*, 2005; Mach *et al.*, 2011; Rudlosky and Fuelberg, 2011; Chronis, 2012; Said *et al.*, 2013; Nastos *et al.*, 2013; Villarini and Smith, 2013; Hutchins *et al.*, 2013; Blakeslee *et al.*, 2014 and references therein].

Interestingly, the enhancement of I_p over the oceans is notably absent for positive polarity CG (+CG) lightning and despite the consistency of this behavior only a handful of studies have tried to determine the physical mechanism responsible [Cooray *et al.*, 2014]. One could categorize the hypotheses addressing the oceanic

©2016. The Authors.

This is an open access article under the terms of the Creative Commons Attribution-NonCommercial-NoDerivs License, which permits use and distribution in any medium, provided the original work is properly cited, the use is non-commercial and no modifications or adaptations are made.

$-I_p$ dominance into three groups: The first group involves hypotheses discussing whether the $-I_p$ oceanic enhancement is a mere artifact [Lyons *et al.*, 1998a; Orville and Huffines, 2001; Said *et al.*, 2013; Zoghoghly *et al.*, 2015]. The second group's focus is on the so-called "attachment process," i.e., the segment within a few meters from the ground where the descending leader and ascending streamer meet [Williams and Heckman, 1993; Williams and Stanfill, 2002; Williams and Heckman, 2011; Williams *et al.*, 2012]. Finally, the third group implicates factors possibly contributing to the thundercloud electric potential [Cooray *et al.*, 2014]. These hypotheses are summarized below.

1.1. Range Effects

The range over which the lightning radio signal propagates can affect the retrieved I_p value. Lyons *et al.* [1998a] suggested that the larger oceanic $-I_p$ values could be attributed to National Lightning Detection Network (NLDN) detection efficiency issues such as the selective detection of CG lying outside the sensor domain (i.e., the ocean), hence of larger $-I_p$ values.

1.2. Propagation Effects

Hypotheses explaining the larger oceanic $-I_p$ values based on the higher electrical conductivity of the (saline) oceanic water have also been discussed [Orville and Huffines, 2001], in the context that this would reduce the propagation attenuation of the lightning-radiated signal, leading to the inference of larger I_p values [Rachidi *et al.*, 2004]. However, this hypothesis has been refuted since it fails to explain the different responses between the CG polarities [Orville and Huffines, 2001; Said *et al.*, 2013].

1.3. CG Attachment Processes

Recent studies have provided ample documentation that the oceanic $-CG$ s not only exhibit larger $-I_p$ values but they are also short-pulsed [Williams, 2006]. The faster abridging between a negative descending CG leader with the upward positive streamer, over a relatively smoother oceanic surface (i.e., as opposed to a rougher land), is suggested to be one of the driving mechanisms explaining the larger oceanic $-I_p$ values [Williams and Heckman, 2011; Williams *et al.*, 2012]. In this context, the *dielectric* relaxation time of the medium that connects the tip of the $-CG$ leader and terminal point (e.g., land/ocean) has also been brought up as a potential contributor to the observed oceanic $-I_p$ enhancement [Williams and Heckman, 1993; Williams and Stanfill, 2002]. For a rapidly descending leader, the relaxation time over the ocean is much shorter than over land due to electrical conductivity. Hence, it would be reasonable to assume that this shorter/faster electric field response over oceanic water, combined with a smoother oceanic surface and the absence of coronae, would further facilitate a faster downward leader and upward streamer attachment process (i.e., the "final jump" as described in Williams [2006]), a faster return stroke hence larger $-I_p$ values [Williams *et al.*, 2012]. Whether spatial variations in salinity (i.e., hence electrical conductivity and relaxation times) might be further contributing to the oceanic $-I_p$ variations is discussed in Cummins *et al.* [2005], Chronis [2012], and later in this paper.

1.4. Thundercloud Potential Enhancement

Processes that enhance the thundercloud electric potential are also expected to produce $-CG$ of larger $-I_p$ values [Cooray and Becerra, 2012]. Orville [1990] contextualized the later by documenting that over the contiguous U.S. (CONUS) the $-I_p$ values increase southwards. That author attributed this to the southward increase of cloud top heights, in the pretext that taller clouds allow more charge storage, thundercloud potential hence larger I_p values. Chauzy and Soula [1999] suggested that in the presence of electric fields, the ground coronae, initiated from tall objects such as trees and buildings, favor the upward transport of positive charge into the lower parts of the cloud, thereby partially contributing to the formation of the lower positive charge center (LPCC). This hypothesis speculates that the limited presence of LPCC suppresses the electrical discharges between the main negative charge in the middle and lower thundercloud levels [Williams, 1989], leading to larger thundercloud potential and larger $-I_p$ values [Cooray and Becerra, 2012; Cooray *et al.*, 2014; Chronis *et al.*, 2015a]. Given the limited presence of coronae over the ocean, the LPCC-related hypothesis is a good fit in explaining corresponding $-I_p$ oceanic enhancement [Williams and Heckman, 1993].

Jayaratne *et al.* [1983] demonstrated experimentally that in the presence of sodium chloride (NaCl) the ice particles deviate from the typical “charge polarity versus temperature” functions originally shown in Takahashi [1978], where in a relatively NaCl-free environment, the heavier precipitating graupel reverses its polarity from negative to positive at higher temperatures. Interestingly, the laboratory experiments by Jayaratne *et al.* [1983] demonstrated that for NaCl concentrations of $\sim 10^{-5}$ normality units or higher and temperatures higher than about -10°C , the graupel does not acquire positive charge but maintains its negative surplus. The NaCl concentrations similar to the ones used in the laboratory experiments by Jayaratne *et al.* [1983] have not only been found in marine clouds by Miller [1974], Khemani *et al.* [1981], and Möller [1990] (e.g., $\sim 1\text{--}2\text{ mg/L}$) but also in rainwater over the continental and coastal U.S. ($>2\text{ mg/L}$ or $\sim 10^{-5}\text{ N}$ [Junge and Werby, 1958]).

Based on the findings by Jayaratne *et al.* [1983], Cooray *et al.* [2014] argued that the presence of NaCl would tend to suppress the LPCC in the storm’s vertical charge distribution (i.e., falling graupel not reversing its sign from negative to positive), effectively reducing the number of $-CG$ thereby leading to larger $-I_p$ values (e.g., see above discussion). In this hypothesis, the expected impact of NaCl on the thunderstorm’s vertical charge structure pertains only to the lower cloud levels and respective charge polarity, thus is not likely to impact the $+I_p$ values [Cooray *et al.*, 2014].

1.5. Role of Aerosols and Condensation Nuclei

Aerosols have been frequently linked to CG activity [Lyons *et al.*, 1998b; Orville *et al.*, 2001; Williams and Stanfill, 2002; Williams *et al.*, 2002; Steiger *et al.*, 2002; Yuan *et al.*, 2011; Kucienska *et al.*, 2012; Fuchs *et al.*, 2015], but an explanation pertinent to the $-I_p$ variation has yet to appear. In a similar context, the relationship between lightning and the presence of ice crystals has been rigorously established [Saunders *et al.*, 2006; Sherwood *et al.*, 2006, and references therein]. Brook [1992, 1995] attributed the larger $-I_p$ values in winter $-CG$ over the U.S. to the increased amounts of solid (i.e., ice) hydrometeors that lead to higher dielectric breakdown thundercloud potential (i.e., larger $-I_p$ values). It has been acknowledged for at least five decades that ice particles over the oceans are larger (by $\sim 8\text{--}10\%$) than over the continents [Wexler, 1960]. The latter fact has recently received ample corroboration from space-based observations by the Moderate Resolution Imaging Spectroradiometer (MODIS) [Platnick *et al.*, 2003]. Along these lines, studies by Avila *et al.* [2002, and references therein] documented something rather intuitive: that larger ice particles transfer more charge during the respective particle collisions in the mixed phase (i.e., in the presence of supercooled water). It could be further assumed that a larger charge transfer effectively increases both the total cloud charge and cloud potential, thereby I_p values [Cooray and Becerra, 2012]. Despite the abovementioned links between lightning flash and ice particle size, a relevant explanation for the $-I_p$ oceanic-continental contrast has not been pursued by the recent literature. This study will explore a multitude of data sets, and to the extent possible, test the previously mentioned hypotheses. To this end, in addition to the CG information, NASA’s MODIS/Terra (for cloud top height and ice crystal size) and Aquarius (for salinity) remote-sensing retrievals are employed in this study, encompassing the CONUS and surrounding oceans.

2. Data and Methodology

2.1. CG Lightning

The National Lightning Detection Network (NLDN) [Cummins *et al.*, 1998] consists of sensors that detect lightning discharges using direction-finding and time-of-arrival techniques. The CG detection efficiency ranges between 90 and 95% over the CONUS, with a median location error less than 500 m [Cummins and Murphy, 2009]. For the I_p retrieval, the NLDN sensors account for groundwave propagation of the radiated electromagnetic field [Cummins and Murphy, 2009; Said *et al.*, 2010; Mallick *et al.*, 2014]. Although these I_p estimates ($\sim 13\%$ mean error) have been demonstrated for only negative subsequent strokes [Mallick *et al.*, 2014], we assume here that the peak radiation fields are also positively correlated with the actual I_p values. The temporal and spatial I_p integrations computed throughout the analysis depend on the size of the CG population. For example, a population of $\sim 10^4$ CG has an I_p standard deviation of 25 kA [Anderson and Eriksson, 1980] and I_p RMS error of ~ 0.25 kA [see Chronis *et al.*, 2015a]. Whenever the results of this analysis are deemed to be sensitive to RMS, the discussion will be qualified appropriately. The analysis is limited to the NLDN

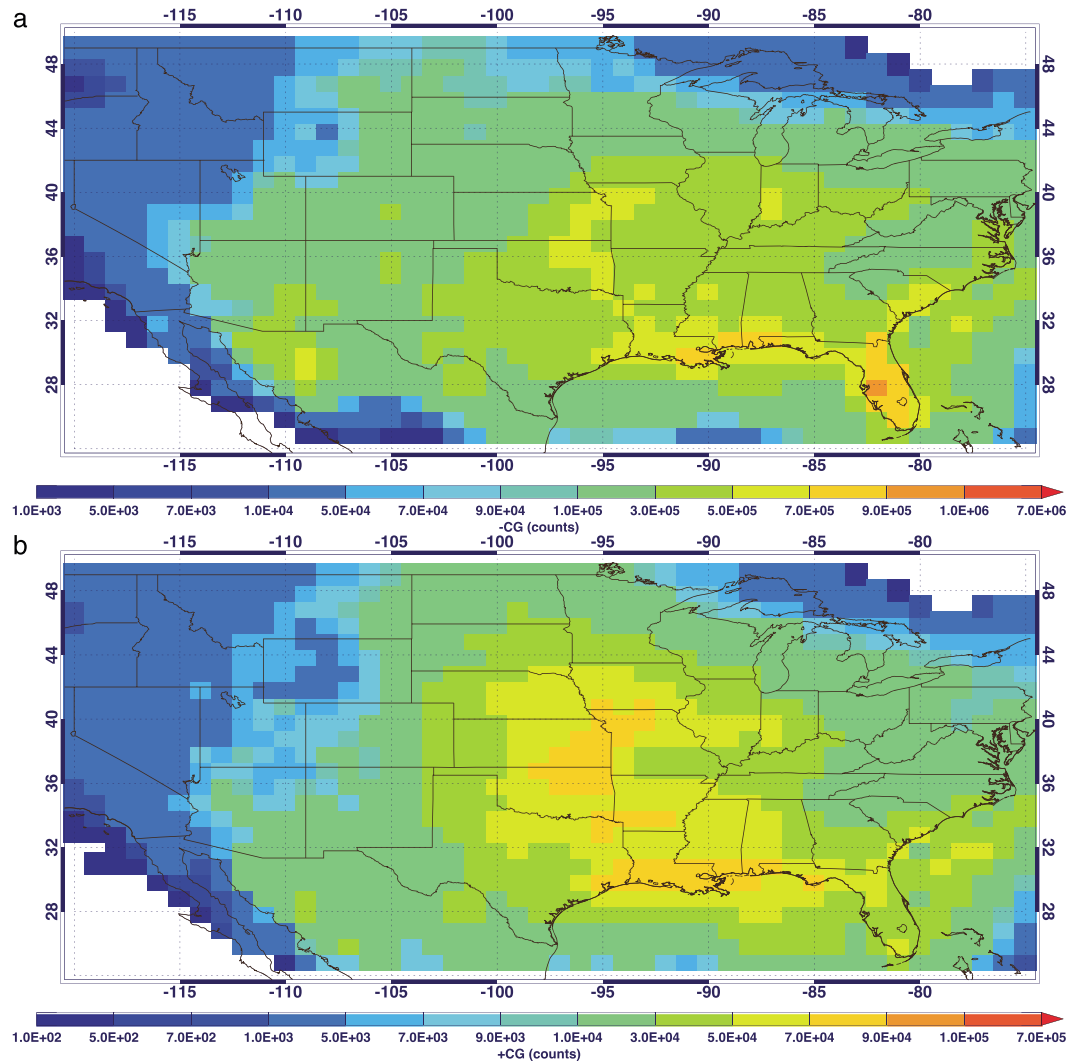


Figure 1. Total (2004–2010) NLDN annual (a) –CG counts and (b) +CG counts at 1° × 1° spatial resolution.

postupgrade period (2004–2010 [Rudlosky and Fuelberg, 2010; Koshak et al., 2015]). The CG polarity identification constraints $I_p < -10$ kA for –CG [Biagi et al., 2007] and $I_p > +15$ kA for +CG [Cummins and Murphy, 2009] are applied. Figures 1a and 1b illustrate the total CG counts for both polarities, and Figures 2a and 2b exemplify the arguments made in the Introduction, by portraying the $-I_p$ transition over the Gulf of Mexico and U.S. East coast, at a spatial resolution of 1° × 1° (Figure 2a). In contrast, the maps for $+I_p$ show no consistent behavior (Figure 2b). Note that the 1° × 1° employed in Figures 1 and 2 is intended only for visualization purposes and the following sections implement a much finer spatial resolution.

2.1.1. Geographical Region Averaging

We compute the total CG counts and respective I_p geometrical means (2004–2010) for four U.S. regions (Figure 3) in 0.25° meridional or zonal increments. These regions encompass (1) 28.75°N to 38.5°N, over the longitudes 90°W to 85°W (Gulf Coast, region 1); (2) 83.5°W to 79.5°W, over the latitudes 27°N to 30°N (Florida peninsula, region 2); (3) 40.0°N to 45.0°N, over the longitudes 88°W to 86°W (Lake Michigan, region 3); and (4) 90.0°W to 74.5°W, over the latitudes 35°N to 38°N (Mid-Atlantic Coast, region 4). The use of zonal and meridional averaging relates to the orientation of the coastline of each respective region. For instance, region 1’s coastline is oriented W-E, so that we study the meridional variation of the zonally averaged quantities. The choice of the geometric mean for I_p is deemed appropriate given the lognormal nature of the respective distribution [Rachidi and Thottapillil, 1993; Said et al., 2013; Chronis et al., 2015a].

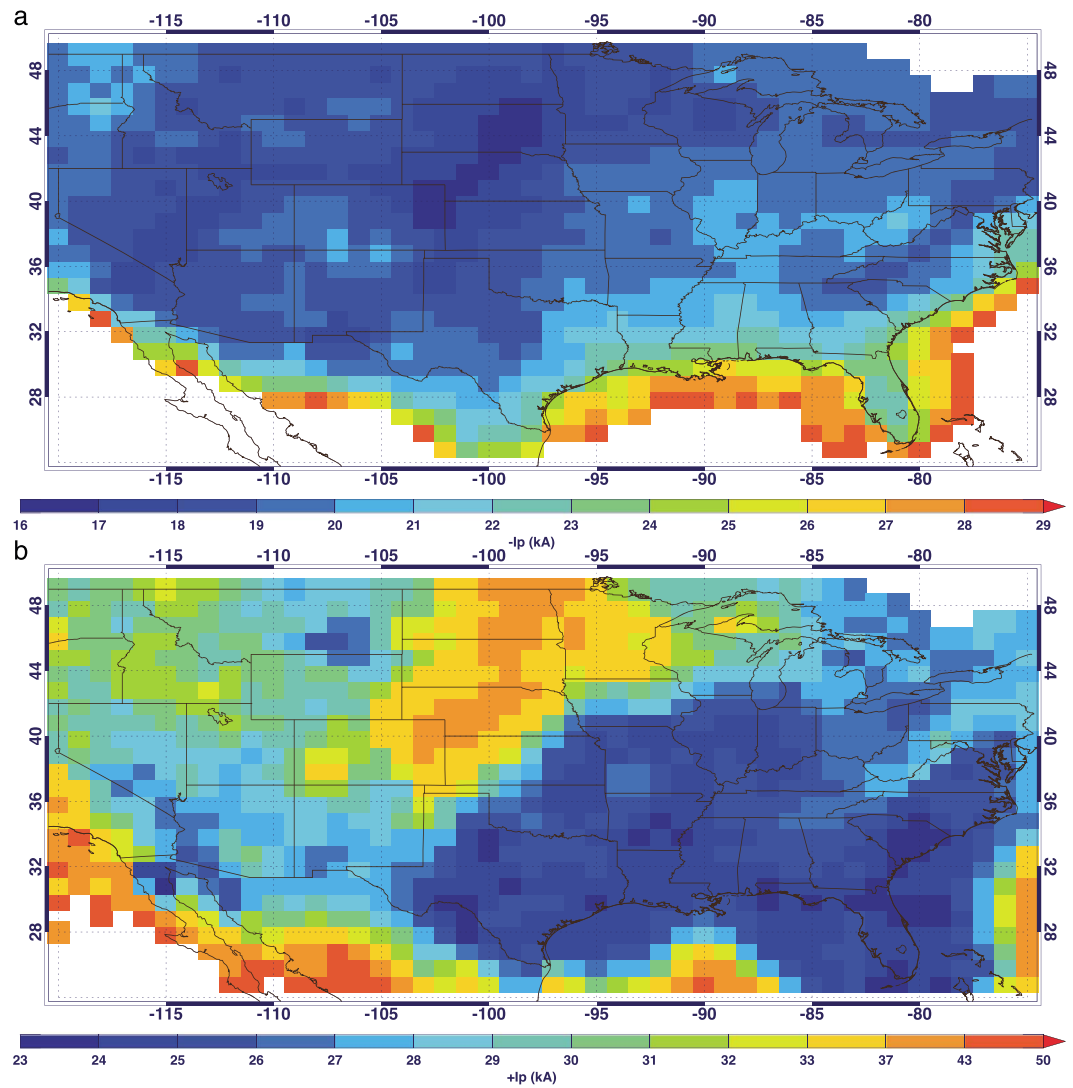


Figure 2. NLDN annual (a) $-I_p$ and (b) $+I_p$ averages (2004–2010) at $1^\circ \times 1^\circ$ spatial resolution.

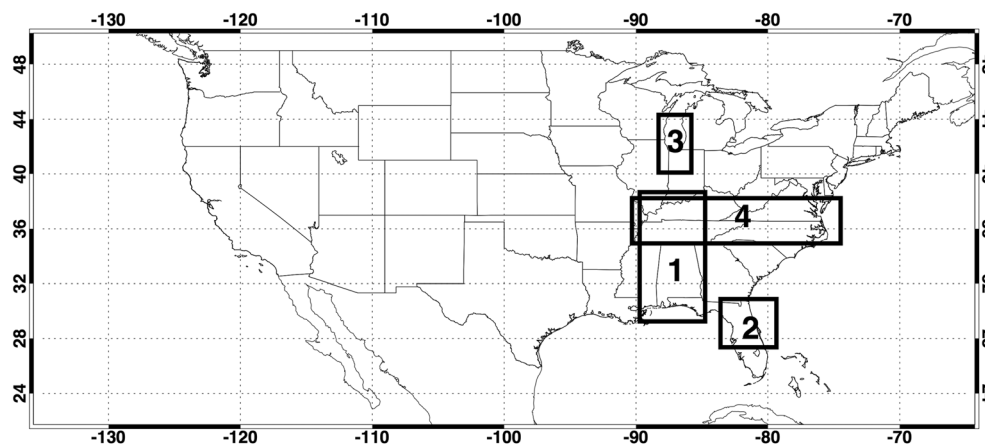


Figure 3. The four regions straddling the CONUS and relate to the latitudinal and longitudinal CG total counts and I_p averages (2004–2010).

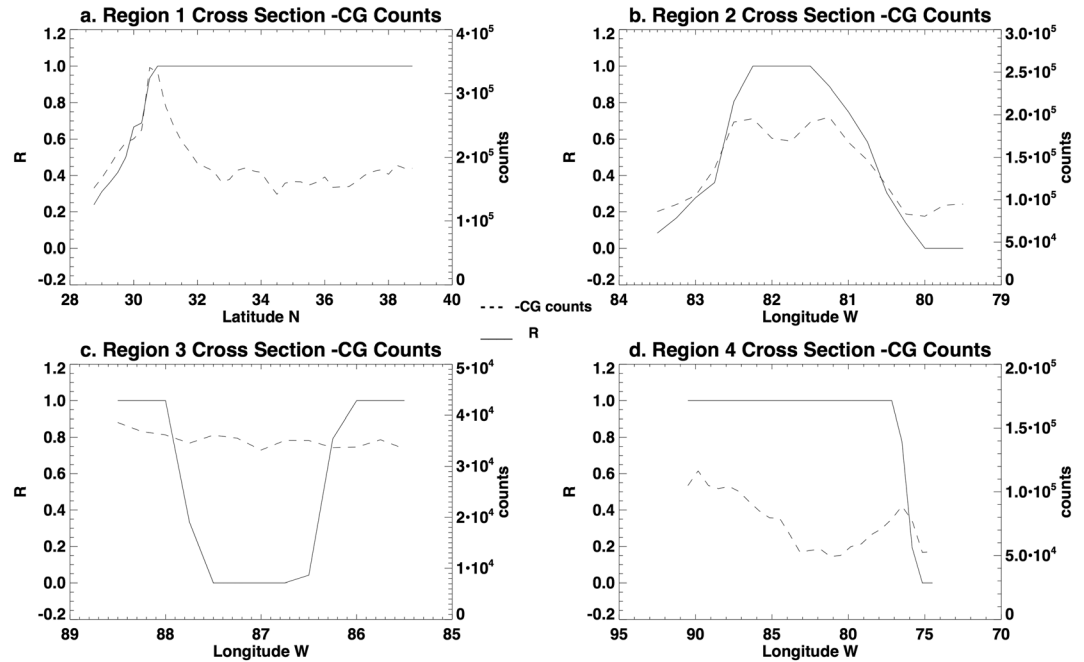


Figure 4. The $-CG$ count (2004–2010) cross sections for regions 1 through 4. Solid line represents R (values range from 0 to 1, with $R = 1$ indicating that all included pixels are continental, left y axis, unitless). Dashed line represents the $-CG$ counts (right y axis). X axis is in degrees (north or west). Cross sections are at 0.25° step (meridional or zonal).

For each region we assign a land mask of the same spatial resolution ($0.25^\circ \times 0.25^\circ$) and calculate the land fraction $R = A_L / (A_L + A_W)$, where A_L and A_W are the areas of land and water within the grid cells comprising each region. Indicatively, the R values for grid cells encompassing only oceanic CG are equal to 0, whereas R values for continental CG are equal to 1. Intermediate R values (i.e., $0 < R < 1$) represent grid

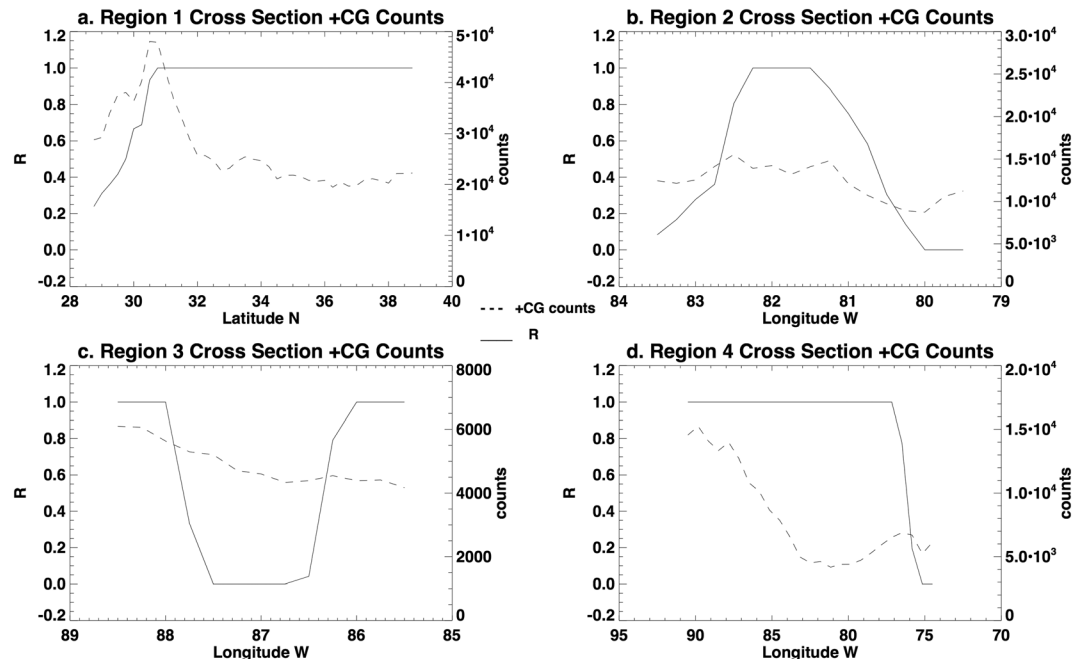


Figure 5. Same as Figure 4, for $+CG$.

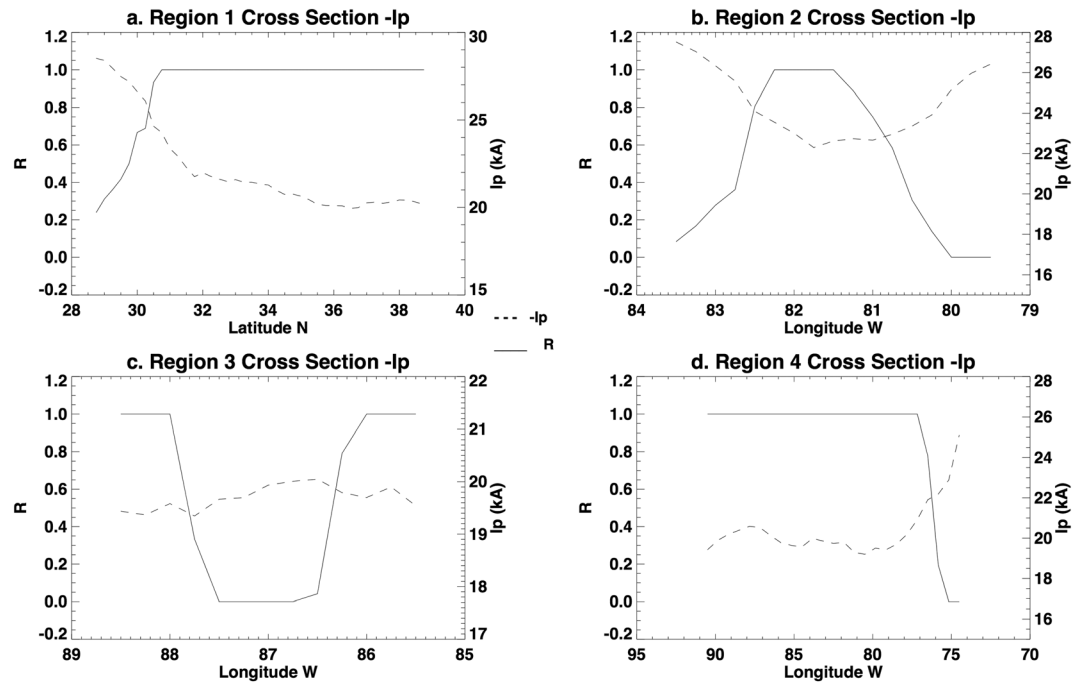


Figure 6. The $-I_p$ average (2004–2010) cross sections for regions 1 through 4. Solid line represents R (values range from 0 to 1, with $R = 1$, indicating that all included pixels are continental, left y axis, unitless). Dashed line represents the $-I_p$ averages (right y axis, kA). X axis is in degrees (North or West). Cross sections are at 0.25° step (meridional or zonal).

cells containing a mix of both environments. This part of the analysis allows the study of the spatially integrated total CG counts and I_p averages for both polarities as a function of the respective R values, for each of the four regions. The results from this analysis are discussed in section 3.1 and illustrated in Figures 4–7.

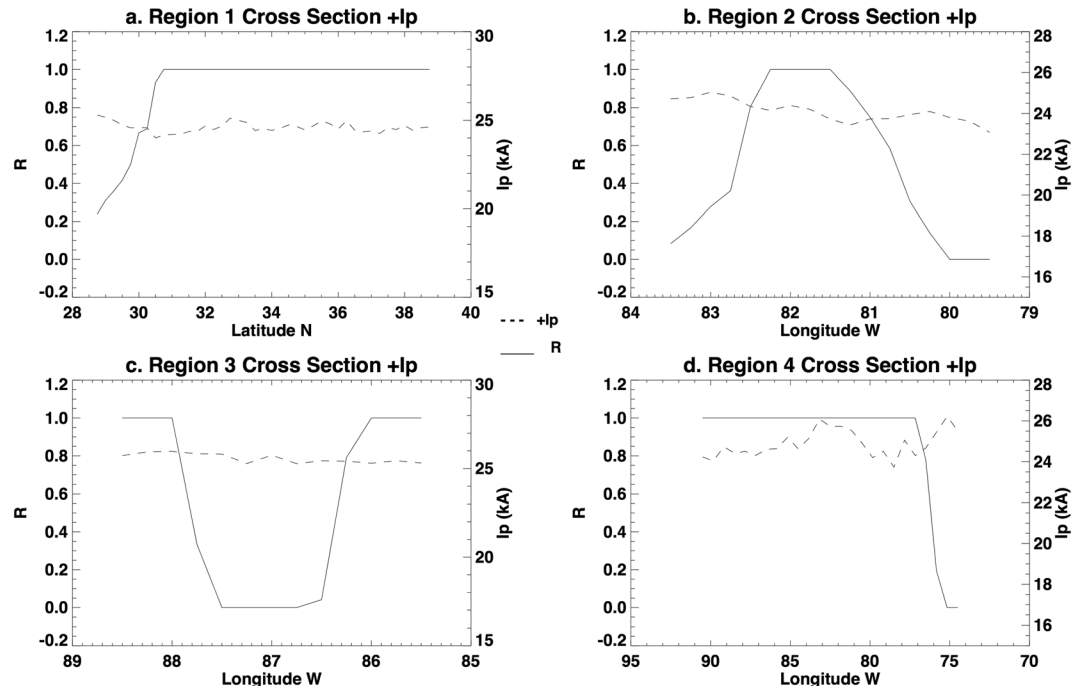


Figure 7. Same as Figure 6, for $+I_p$.

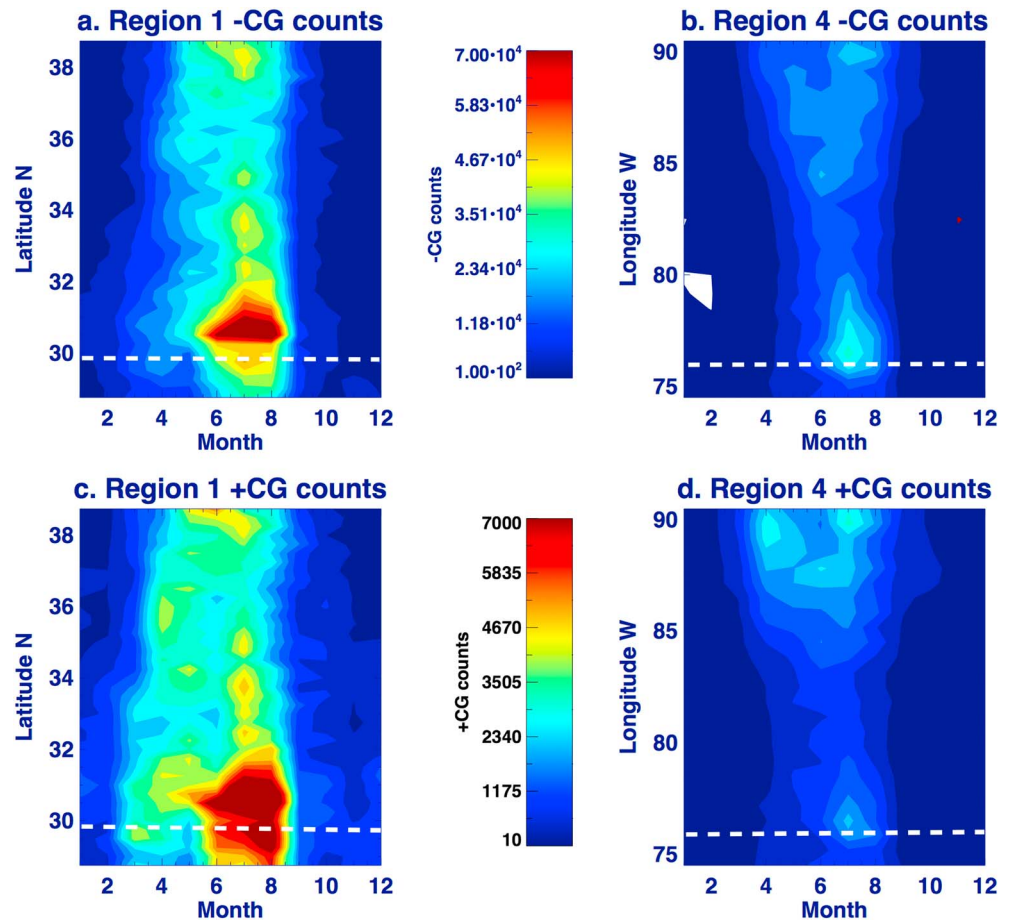


Figure 8. Seasonal (2004–2010) Hovmoller (time-space) plots for –CG counts for regions (a) 1 and (b) 4 and +CG counts for regions (c) 1 and (d) 4. Dashed white line represents the approximate location of the respective coastline for regions 1 and 4. Spatial cross sections are at 0.25° step (meridional or zonal).

2.1.2. Seasonal I_p Variation Across the Oceanic-Continental Boundary

The analysis described in section 2.1.1 is performed for each monthly average (2004–2010) to examine seasonality. Given the additional dimension (i.e., time), we simplify the analysis by emphasizing on the seasonal CG counts and I_p averages for regions 1 and 4 and omitting the R values, since their respective coastlines are approximately parallel to $\sim 30^\circ\text{N}$ and 76°W , respectively. The results from this analysis are discussed in section 3.2 and illustrated in Figures 8 and 9.

2.2. MODIS Ice-Cloud Effective Radius and Cloud-Top Pressure

The Level-3 monthly MODIS products (abbreviated as *MOD08_M3*, for Terra) are acquired from NASA’s Giovanni (version 3.X) online portal, from which we construct time (monthly)-space (*Hovmoller*) climatological averages (2004–2010) for the ice particle effective radius (R_{ice} in micrometer) and cloud top pressure (C_{pr} in pascal, day and night product) at their nominal spatial resolution ($1^\circ \times 1^\circ$) for regions 1 and 4. Both C_{pr} and R_{ice} are products based on the combination of visible and infrared radiation intercepted by the MODIS channels [Menzel *et al.*, 2008], and they represent adequate proxies for the actual ice crystal size and cloud top heights (i.e., higher (lower) C_{pr} , lower (higher) cloud top height given a standard atmosphere [Platnick *et al.*, 2003; King *et al.*, 2004]). All visible/infrared remote-sensing cloud retrievals are not representative of the entire atmospheric column but rather the cloud tops. Despite this inherited uncertainty it would be reasonable to assume that if the average R_{ice} in region A (cloud top) is greater than R_{ice} in region B (cloud top), then sedimentation processes (i.e., finer (coarser) particles at higher (lower) altitudes) enforce the same relationship at altitudes below the cloud top. This assumption pertains to the discussion in section 4.6.

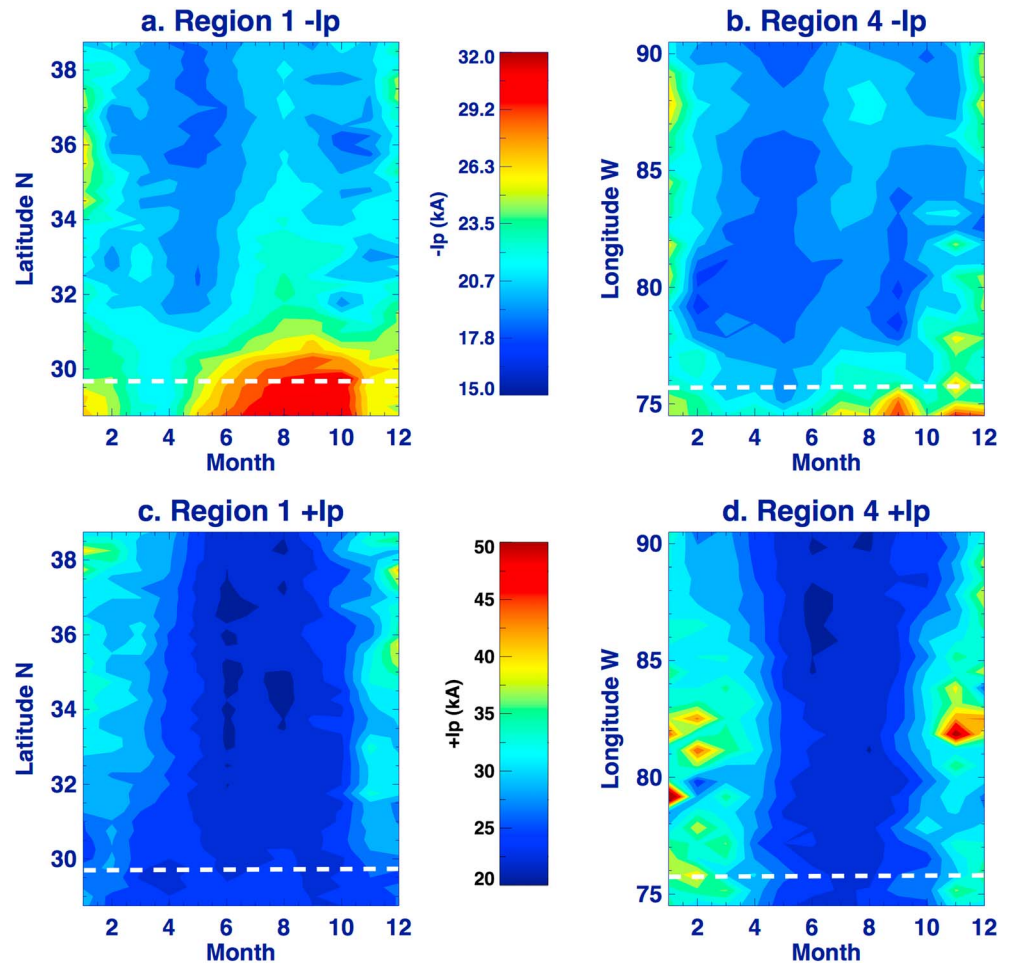


Figure 9. Same as Figure 8, for $-I_p$ and $+I_p$.

2.3. Aquarius Sea Surface Salinity

NASA's Earth System Science Pathfinder Aquarius mission offers the first space-based global observations of sea surface salinity (SSS, in practical salinity unit (psu) dimensionless, i.e., g/kg), from a synchronous polar Earth orbit. The SSS retrievals (accuracy ~ 0.2 psu) are based on the principle that emission in the microwave spectrum decreases as SSS increases, but additional corrections are applied in the basic radiometric observations during postprocessing [Meissner and Wentz, 2004]. Aquarius maps the global ocean surface salinity with a spatial resolution of ~ 100 – 150 km. We obtained the Level-3 monthly SSS data from NASA's Jet Propulsion Laboratory and constructed time-space averages for 2013–2014 given that Aquarius is a relatively newer mission thus it encompasses a shorter period than Terra/MODIS.

3. Results

3.1. Cross Sections for CG and I_p

Figures 4a–4d illustrate the cross sections of the total $-CG$ counts for regions 1–4. Figures 4a and 4b demonstrate a clear maximum for the $-CG$ counts near the respective coastlines, Figure 4d demonstrates an overall increase in $-CG$ counts as we move inland, whereas Figure 4c demonstrates a rather invariant $-CG$ count behavior across the land-fresh water interface. This dominance in continental lightning activity is well documented in numerous studies [see Changnon, 1988; Pinto et al., 1996; Orville and Huffines, 2001; Christian et al., 2003; Rivas Soriano et al., 2005; Chronis et al., 2006; Chronis, 2012; Nastos et al., 2013; Holle, 2014, and references therein]. The localized CG count maximum found along the coastlines likely relates to the convective processes driven by the land-sea breeze circulation [Arritt, 1993] (e.g., see Figures 4a and 4d). The absence

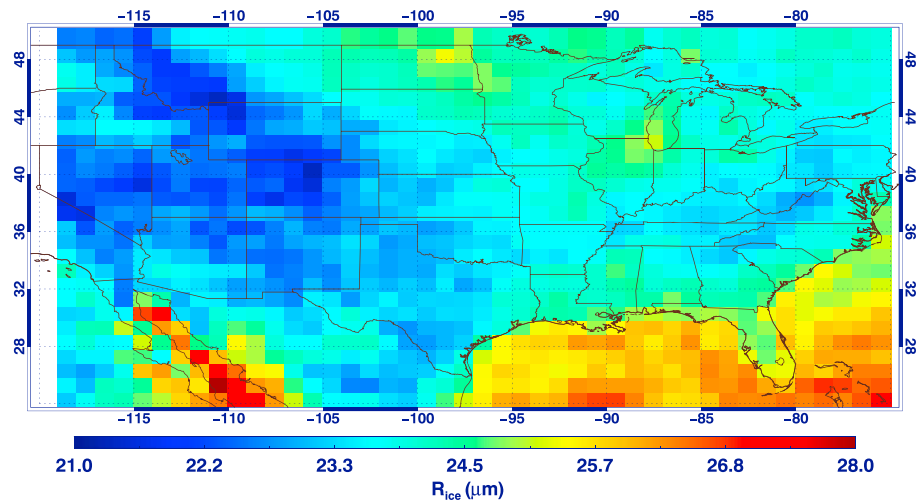


Figure 10. Climatological average (2004–2010) for MODIS R_{ice} at $1^\circ \times 1^\circ$ spatial resolution.

of similar behavior over region 3 (Figure 4c) is likely due to the limited size of the water body encompassed (Lake Michigan) and the dominance of the zonally propagating migratory storm systems during the warm season. Figures 5a–5d illustrate the cross sections of the total +CG counts for regions 1–4. Considerable consistency is apparent between the CG counts for both polarities, if one accounts for the well-established fact that the +CG counts are ~ 1 order of magnitude less than the respective $-CG$ counts [e.g., see Orville and Huffines, 2001; Koshak et al., 2015].

Figures 6a–6d illustrate the cross sections of the $-I_p$ spatial averages for regions 1–4. Figure 6a reveals a northward gradual $-I_p$ reduction (i.e., in absolute values) that closely mirrors the increasing R values in region 1. This inverse relationship is most evident across the main coastline of region 1, where there is an I_p gradient of ~ 2 – 2.5 kA between $\sim 29.5^\circ\text{N}$ and 30.5°N that gradually disappears further inland (e.g., north of $\sim 31.5^\circ\text{N}$). The highlighted $-I_p$ and R spatial co-variation is even more pronounced in region 2 (Figure 6b), where the cross section traverses the Florida peninsula from west-to-east, encompassing successive water-land-water environments. Across region 2's western coast (i.e., between $\sim 82.8^\circ\text{W}$ and 82.2°W) the $-I_p$ values reduce by ~ 2 – 2.5 kA. Similarly, across the eastern coast of region 2 (81.5°W to 80.5°W) the $-I_p$ values increase by approximately the same amount (Figure 6b). The overall $-I_p$ reduction for regions 1 and 2 along the respective cross sections ranges between ~ 6 and 7 kA (Figures 6a and 6b). Interestingly, the $-I_p$ values exhibit no such gradients across the continental-fresh water coast (region 3; Figure 6c), while any changes in $-I_p$ values within region 3 appear to be statistically insignificant (see section 2.1). This is an important finding in our study and stands in agreement with Lyons et al. [1998a] and Cummins et al. [2005]. The relationship between R and $-I_p$ for region 4 (Figure 6d) falls into the same category as regions 1 and 2.

Figures 7a–7d illustrate the cross sections of the $+I_p$ spatial averages for regions 1–4. In sharp contrast with the $-I_p$ (Figures 6a, 6b, and 6d), the $+I_p$ cross sections for all regions fail to exhibit any clear relationships with the respective R values (Figures 7a–7d).

3.2. CG and I_p Hovmoller Analysis

The time-space (Hovmoller) plots of the total monthly $-CG$ counts for regions 1 and 4 are illustrated in Figures 8a and 8b, findings that highlight the well-documented seasonal surplus of lightning activity over the continents during warmer months. The summertime $-CG$ count maximization is observed within $\sim \pm 1^\circ$ of the main coastline of regions 1 and 4 (represented by the white dashed line, see Figures 8a and 8b). Note that the abovementioned $\sim \pm 1^\circ$ might be an overestimate caused by the applied spatial resolution. This feature likely pertains to the enhanced land-sea breeze circulation, especially during the typical warm-season months [Arritt, 1993]. For regions 1 and 4 the seasonal +CG count variation (Figures 8c and 8d) is somewhat similar to the $-CG$ (see Rudlosky and Fuelberg [2011] for similarities with regions 1 and 4), but further highlights a relative +CG enhancement during the months of March–May across the eastern U.S. Great Plains (Figures 8c and 8d; see Figure 12 in Zajac and Rutledge [2001]).

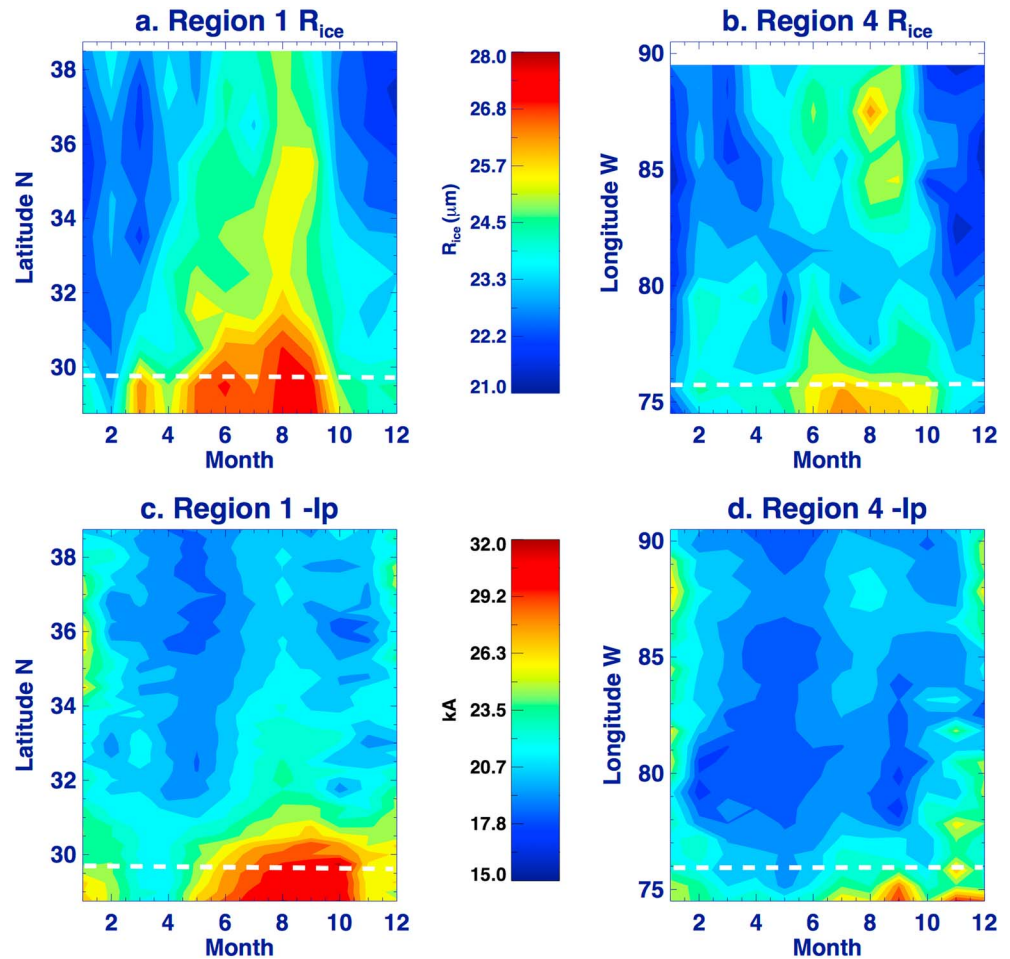


Figure 11. Seasonal (2004–2010) Hovmoller (time-space) plots for MODIS R_{ice} for regions (a) 1 and (b) 4 and $-I_p$ averages for regions (c) 1 and (d) 4. Dashed white line represents the approximate location of the respective coastline for regions 1 and 4. Spatial averaging for MODIS is $1^\circ \times 1^\circ$ and for I_p is $0.25^\circ \times 0.25^\circ$.

Figures 9a–9d are similar to Figures 8a–8d, but for the $-I_p$ and $+I_p$ time-space averages for regions 1 and 4. For region 1, as one moves southwards from latitude $\sim 31.5^\circ\text{N}$, we observe that the $-I_p$ values gradually increase however, this meridional enhancement is more prominent from June through October (Figure 9a). For region 4, we still observe larger $-I_p$ values over the ocean but the respective variation does not exhibit as clear a temporal-spatial clustering as in region 1 (Figure 9b). The temporal-spatial $+I_p$ variation for regions 1 and 4 (Figures 9c and 9d) is vastly different from the respective $-I_p$ (Figures 9a and 9b). In particular, the $+I_p$ values do not demonstrate any oceanic enhancement however, they clearly exhibit larger (lower) smaller during the winter (summer) months with no consistent spatial (meridional or zonal) dependence.

3.3. {Ice Crystal Size, Cloud Top Pressure, and Salinity} Versus I_p Temporal-Spatial Analysis

Figure 10 illustrates the averaged R_{ice} for the period 2004–2010 (same as in Figures 2a and 2b). Besides, the fact that R_{ice} oceanic values are larger than the respective continental (by $\sim 10\%$ on average), a key observation is gleaned from the well-defined contrast along the U.S. coastline. In general, the larger R_{ice} values in Figure 10 reflect the seasonal precipitation patterns (e.g., such as the monsoons over Baja California [see King et al., 2004]). For consistency with the previous Hovmoller analysis, we repeat the computations that resulted in Figure 9, this time accounting for R_{ice} . Figures 11a and 11b illustrate the monthly time-space averages for R_{ice} for regions 1 and 4, while Figures 11c and 11d are the same as Figures 9a and 9b (at the initial 0.25° resolution applied to NLDN). In region 1, we observe a temporal-spatial coherence between the relatively larger R_{ice} values and the respective $-I_p$ enhancement (Figures 11a and 11c). More importantly, we

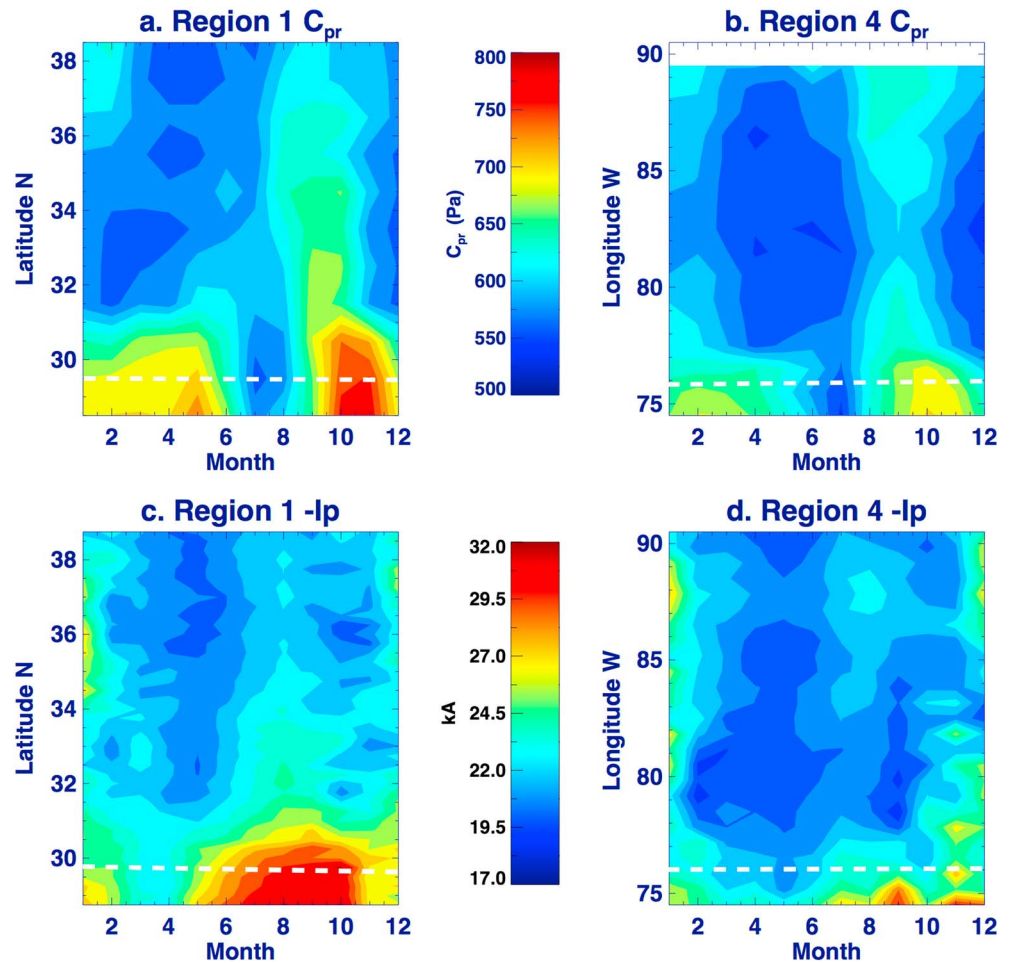


Figure 12. Seasonal (2004–2010) Hovmoller (months-latitude) plots for MODIS C_{pr} for regions (a) 1 and (b) 4 and $-I_p$ averages for regions (c) 1 and (d) 4. Dashed white line represents the approximate location of the respective coastline for regions 1 and 4. Spatial averaging for MODIS is $1^\circ \times 1^\circ$ and for I_p is $0.25^\circ \times 0.25^\circ$.

observe that the R_{ice} temporal-spatial variations capture part of region 1's (Figure 11a) $-I_p$ latitudinal dependence from June to October (Figure 11c). For region 4, some additional temporal-spatial agreement is demonstrated between the two variables in that, the lower $-I_p$ values (Figure 11d) are accompanied by relatively lower R_{ice} values (Figure 11b).

The Hovmoller plots for C_{pr} reveal known climatological cloud top height properties of the oceanic and continental environments (Figures 12a and 12b). As we move closer to region 1's coastline we observe the transition from the winter lower cloud top s (i.e., higher C_{pr}) to the higher cloud tops of the main convective (summer) season (i.e., lower C_{pr}), reverting back to the lower cloud top s in the fall season (Figure 12a). A similar behavior is noted for region 4, although given the C_{pr} meridional averaging, the seasonal variation is somewhat damped (Figure 12b). The comparison between C_{pr} and $-I_p$ Hovmollers (Figures 12c and 12d) fails to exhibit any coherency in the context that the prominent $-I_p$ temporal-spatial variation clearly encompasses both summer and fall seasons (i.e., both low and high cloud top heights).

Figure 13 illustrates the SSS Hovmoller plot for region 1 (at $1^\circ \times 1^\circ$ spatial resolution). Also, note that the averaged latitudes extend from 17°N to $\sim 30^\circ\text{N}$, i.e., the location of the region 1's coastline). The main observation to be gleaned from Figure 13 is the SSS reduction over southern latitudes from June to October. This coastal SSS reduction is likely driven by the increased discharge of the Mississippi River due to precipitation input from the typically wet season of region 1 (i.e., the convective summer season from June through August, followed by the more stratiform season from September through October). Further comparison with the

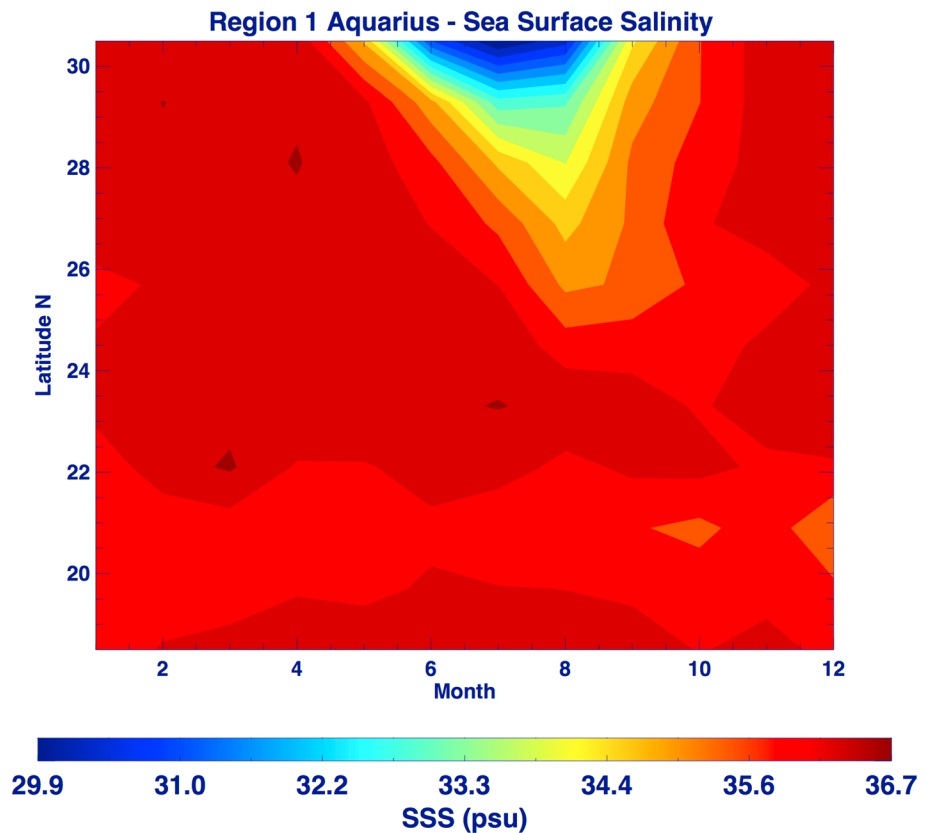


Figure 13. Seasonal (2013–2014) Hovmoller (time-space) plots for SSS for region 1.

respective $-l_p$ Hovmoller for region 1 suggests that as SSS decreases, the $-l_p$ values increase (e.g., see Figure 11c). More detailed discussion on the implications of this finding, in relation to the l_p temporal-spatial variation, is extended in section 4.3.

4. Discussion

The findings of the analysis pertaining to lightning flashes (i.e., CG and l_p) can be summarized as follows:

1. A robust inverse relationship is observed between the $-l_p$ and R across only the oceanic-continental boundaries (regions 1, 2, and 4) but is absent across the continental-fresh water boundary (region 3). This is demonstrated by the gradual $-l_p$ decrease as one approaches the respective coastlines from the ocean.
2. The $+l_p$ spatial variation across all boundaries is unrelated to R .
3. Region 1 reveals a strong seasonal and latitudinal dependence of $-l_p$, with the maximum $-l_p$ values clustered around the summer-early fall months over the southernmost latitudes. This $-l_p$ latitudinal dependence becomes diluted as one moves inland (i.e., northward), with a weaker winter maximum and a less evident minimum in $-l_p$ values for regions 1 and 4.
4. Compared to region 1, region 4 exhibits a less robust $-l_p$ temporal-spatial variation, although it still exhibits larger $-l_p$ values over the ocean during the summer-early fall months.
5. As highlighted in finding 2, no oceanic influence on the $+l_p$ is observed and the temporal-spatial variation for $+l_p$ is similar for both regions 1 and 4. Wintertime $+l_p$ are also dominant across continental environments for both regions (also see finding 3).

The findings of the analysis pertaining to ice effective radius, cloud top pressure and salinity (i.e., R_{ice} , C_{pr} , and SSS) as functions of $-l_p$ values can be summarized as follows:

6. As the $-I_p$ in finding 3, R_{ice} also shows a strong latitudinal dependence with its maximum values clustered around the summer through early fall months over the southernmost latitudes. Across this time-space window, one can argue that the two parameters $\{R_{ice}, -I_p\}$ exhibit a noteworthy degree of coherence.
7. No consistent temporal-spatial coherence is observed between $\{C_{pr}, -I_p\}$ in either region.
8. The lowest SSS values are in phase with the highest $-I_p$ values over the coastal part of region 1.

The novelty of finding 3 stems from the fact that it revisits the argument according to which “the $-I_p$ values are larger over the ocean than the continent.” Instead, the Hovmöller analysis concludes that this argument should be framed as “the $-I_p$ values are larger over the ocean than the continent, a contrast that is blurred across the coastline but also depends on latitude and season.” More importantly, finding 3 is only in partial agreement with the earlier study by *Orville and Huffines* [2001], where these authors documented a clear preponderance of larger $-I_p$ values during the winter months and a minimum over the CONUS during March–April (see Figure 16 in *Orville and Huffines* [2001]). In line with *Orville and Huffines* [2001], region 1 indeed exhibits larger $-I_p$ values during the winter only across the northern CONUS latitudes, but as one moves closer to the region 1’s coastline, it is the summer-early fall months that exhibit the maximum seasonal $-I_p$ values. This apparent contradiction to the reports by *Orville and Huffines* [2001] could be ascribed to the fact that those authors did not explicitly examine latitudinal $-I_p$ averages. The $-I_p$ latitudinal dependence established herein was originally implied in *Orville* [1990] however, that analysis did not report any temporal-spatial averages. In the context of finding 3, the $-I_p$ latitudinal dependence partially supports the observations in *Orville* [1990], according to which larger $-I_p$ values are observed as latitudes decrease, but only when one considers the typical (northern hemisphere) warmer months.

Findings 3 and 4 are also in accordance with the $-I_p$ continental dominance during winter months reported in *Brook* [1992, 1995], *Orville and Huffines* [2001], and others [e.g., *Rivas Soriano et al.*, 2005; *Rudlosky and Fuelberg*, 2011; *Chronis*, 2012; *Nastos et al.*, 2013; *Villarini and Smith*, 2013; *Hutchins et al.*, 2013, and references therein]. Finally, in terms of finding 5 we observe consistently larger $+I_p$ values during the typical winter months, in agreement with previous studies over the CONUS [e.g., see *Orville and Huffines*, 2001] and worldwide [*Rivas Soriano et al.*, 2005; *Chronis*, 2012; *Nastos et al.*, 2013].

One could further make a simplistic argument according to which, a controlling factor of I_p is the CG counts. From this viewpoint, a reduced frequency of the CG discharges should further increase the electrostatic charge accumulation, which would lead to larger I_p values (also discussed in *Cooray et al.* [2014]). This inverse relationship has been shown to partially exist on a diurnal (local time) scale across CONUS and Brazil [*Chronis et al.*, 2015a, 2015b]. Therein, the authors suggest that the weaker, less turbulent morning updrafts promote larger distances between opposite charge centers leading to larger $-I_p$ values [*Chronis et al.*, 2015a], which in this context it could be argued that higher (lower) CG counts relate to increased (decreased) turbulent regimes. However, the temporal and spatial scales implicated herein do not support such dependence. For instance, region 1 demonstrates maximum $-CG$ counts just on the land-side of the oceanic-continental boundary (Figure 4a), including part of the $-I_p$ enhancement near the coastline (Figure 6a). In addition, while the $+CG$ counts follow the same spatial trend as the $-CG$, the corresponding $+I_p$ values remain practically unchanged across the coastal boundary. More importantly, any $-CG$ count versus $-I_p$ dependence is further disputed if one considers that the larger $-I_p$ values encompass the entire wet season of region 1 but in contrast the maximum $-CG$ counts encompass from June to August (see Figures 8a and 9a).

Next we discuss how the aforementioned findings could be further considered as supporting or refuting evidence for the various hypotheses discussed in the previous sections.

4.1. Assessing the Range Effect

Because several of the preceded computations include CG detected ~ 75 – 100 km from the respective coastline (especially in regions 1, 2, and 4), it could be questioned if NLDN is prone to selectively detect the CG farther from the network’s sensors hence of larger I_p values [see *Mallick et al.*, 2014]. For instance, the $-I_p$ reduction observed in region 1 (Figure 6a) along $\sim 28.75^\circ\text{N}$ to 30.25°N could be partly attributed to the distance of these flashes from the NLDN sensors that are lined up along the coast of Louisiana, Mississippi, Alabama, and Florida (not shown). Beyond ~ 200 km, NLDN fails to detect low I_p discharges [*Mallick et al.*, 2014]. The methods employed in this study cannot fully decouple the $-I_p$ reduction solely associated with variations in the NLDN detection efficiency. Nevertheless, the fact that the $+I_p$ exhibit no trend similar to the $-I_p$

(e.g., Figures 7a and 7b), in combination with the gradual transition of $-I_p$ values across the respective coastlines (e.g., Figure 6), supports the notion that the oceanic-continental $-I_p$ contrast is cannot be attributed to detection efficiency. This result is also supported by recent studies [Said *et al.*, 2013; Zoghzoghy *et al.*, 2015].

4.2. Assessing Effects Related to Signal Propagation

Finding 2 (see Figure 5) shows that the coastal $-I_p$ transitions are less abrupt than R , so any hypothesis relating the electrical conductivity and signal propagation processes (e.g., signal attenuation/gain) also cannot explain this observation [Said *et al.*, 2013; Cooray *et al.*, 2014]. Furthermore, if surface electrical conductivity/signal propagation artifacts were at play, then these would also affect the associated $+I_p$ values (Figure 7), contrary to finding 2. Similar discussion is extended in Orville and Huffines [2001] and Cooray and Rakov [2011].

4.3. Assessing Effects Related to Attachment Processes

Findings 1 and 3 document a gradual transition to larger (smaller) $-I_p$ values on the ocean (land) side of the oceanic-continental boundary but no change across the continental-fresh water boundary. Williams [2006] and Williams *et al.* [2012] discuss that the faster propagating negative leaders are more likely to close the gap quickly in the final jump connecting with the upward propagating streamer, especially over a relatively smoother oceanic surface, consequently leading to more charge being deposited along the leader and neutralized by the return stroke. Moreover, given the documented “slower final jump” of positive leaders [Williams, 2006], the role of attachment process could also be supportive of the fact that $+I_p$ do not exhibit oceanic enhancement, in line with finding 2. This is also in agreement with field observations by Zoghzoghy *et al.* [2015], who suggest that attachment processes and the differences in electrical properties between land and ocean might be contributing to the observed oceanic $-I_p$ enhancement. However, if attachment processes were the dominant mechanism then this assumption should have been accompanied by a more abrupt $-I_p$ change (e.g., similar to a step-function) across the ocean-continent boundary. The latter is not corroborated by the observations herein. Nevertheless given the fundamental differences of electrical properties between the two media (e.g., conductivity and relaxation times) and in conjunction with the different temporal/spatial scales implicated in this study, it would be reasonable to suggest that these processes might partially contribute to the observed $-I_p$ contrast.

4.4. Assessing Coronea Effects

The reported findings might raise questions as to whether the corona mechanism could be a primary contributor to the $-I_p$ oceanic enhancement. As previously discussed, the gradual $-I_p$ enhancement versus the more abrupt R values changes (see Figure 6) provides clues that the dominant mechanism might lie beyond a strict environmental boundary (also discussed in section 4.3). Moreover, on the premise that fresh water and oceanic surfaces should both suppress the coronea generation, the $-I_p$ enhancement ought to be present over both surfaces, in direct contrast with finding 1. More complex candidate mechanisms could also be speculated from the perspective that the wind-induced sea-spray generation [see Reiter, 1994] or precipitation splashing on the ocean surface could effectively generate space charge especially during the wet season (e.g., Worthington jets [Gathman and Trent, 1968; Muir, 1977; Rein, 1996]).

4.5. Assessing the NaCl Effect

Findings 1 and 3 strongly suggest that the $-I_p$ might depend on some property that is ubiquitous over the oceanic environment but is unrelated to the I_p retrieval/signal propagation (see sections 4.1 and 4.2). More importantly, findings 1 and 3 also depict a blurred spatial I_p transition, but a transition that additionally exhibits a pronounced temporal variation. This evidence suggests that a possible controlling factor pertains to a larger-scale process, without denying the possible simultaneous contribution of smaller-scale mechanisms such as the attachment processes discussed in Williams *et al.* [2012] (see section 4.3). The postulation in Cooray *et al.* [2014] is consistent with the fact that the anticipated NaCl impact should be effective over oceanic but not fresh water environments, exclusively for the $-CG$, in line with our findings (e.g., finding 2). Moreover, Cooray *et al.* [2014] is in further agreement with the latitudinal $-I_p$ distribution (see Figure 9 a), if one considers that processes such as the land-sea breeze enable the NaCl transport inland [e.g., see Arritt, 1993; Lewandowska and Falkowska, 2013].

However, the demonstrated temporal-spatial $-I_p$ variation (see Figure 9a) raises a few interesting questions in regard to whether the NaCl mechanism can be identified as the sole controlling factor of the oceanic $-I_p$ enhancement. These are as follows: (1) If NaCl is overall reducing the number of $-CG$ counts (due to the postulated reduction of LPCC [see Cooray *et al.*, 2014]) then why do Figures 8a and 9a indicate that there is a temporal-spatial overlap between the larger $-I_p$ values and higher $-CG$ counts? (2) How can the NaCl mechanism explain the temporal-spatial variation exhibited by the $-I_p$ values? Besides, the fact that the implemented laboratory and thundercloud NaCl concentrations are similar (see section 1.4), we do not have explicit knowledge of how these vary on a seasonal basis. Yet it would be reasonable to expect that higher NaCl concentrations in the thundercloud are temporally coincident with the stronger updrafts during the typical summertime convection (see maximum CG counts; Figure 8a) and transported via processes such as surface-layer entrainment of wind-induced sea-spray [Blanchard, 1989; Rosenfeld *et al.*, 2002]. Conversely, our evidence (finding 3; Figure 9a) demonstrates a clear $-I_p$ enhancement that extends beyond the typical summer season (i.e., ending in approximately October), which begs the question “how can the NaCl mechanism explain the larger $-I_p$ values beyond the summertime convection?” At this point we explore the scenario where higher sea surface NaCl concentrations (i.e., higher SSS), which under the assumption of e.g., raindrop splashing or transport of salt particles aloft [Rein, 1996], would also promote higher NaCl concentrations aloft. Again in this case, additional problems arise in the context that the period of enhanced $-I_p$ values in region 1 coincides with the lowest SSS values (finding 8; Figure 13), hence presumably lower NaCl concentrations aloft. Based on the discussion extended in section 1.3, this finding might present itself as counterintuitive, but also contradictory to the findings in Chronis [2012]. Nonetheless, it is important to emphasize that this finding casts doubt on the role of salinity variations in regulating the oceanic $-I_p$ variations and not the role of the electrical conductivity differences between land and ocean in regulating the respective $-I_p$ contrast (see section 1.3).

Interestingly, the apparent discrepancy between SSS and $-I_p$ has provided the analysis with further important clues. First and foremost, this seasonal SSS coastal decrease likely relates to the “wet” season of region 1, where the surplus of precipitation increases the fresh water discharge from the Mississippi River and other streams entering the Gulf of Mexico. It is important to underscore that this SSS decrease is a strictly local/coastal effect and does not imply that, in general, global SSS variations are simply regulated by the precipitation input. Moreover, the wet season also hints for increased availability of atmospheric moisture, which also strongly regulates ice properties in thunderclouds. In retrospect, it has been the SSS- I_p -related finding (finding 8) that led the analysis in hand to the inclusion of the MODIS data. This is what we discuss next.

4.6. Assessing R_{ice} and C_p Effects

Studies confirm that the growth of larger ice crystals is favored in environments with higher mixing ratios of atmospheric water vapor [Duda *et al.*, 2002; Rädcl *et al.*, 2003]. In this context, the observed R_{ice} seasonal enhancement during the months of June through October likely relates to the increased atmospheric water vapor availability promoted by the higher sea surface temperatures during the typical wet season of region 1. The temporal-spatial coherence between R_{ice} and SSS (see Figures 11a and 13), at least over the coastal region 1, supports this argument. More importantly, finding 6 highlights an additional temporal-spatial coherence, namely that between R_{ice} and $-I_p$ (also shown in Figures 11a and 11c), which constitutes an important clue in the effort to understand at least part of the observed $-I_p$ land/ocean contrast. Although the demonstrated temporal-spatial coherence between Figures 11a and 11c does not establish causality, the strong physical links between ice particle size and lightning occurrence suggest that a possible mechanism controlling part of the $-I_p$ temporal-spatial variations observed across the oceanic-continental boundary might be ascribed to the variations in R_{ice} .

While the strongest advocates for the R_{ice} candidacy are the robust physical linkages to lightning physics and the observed temporal-spatial coherence with $-I_p$, this hypothesis is also not invincible. We observe that the overall R_{ice} difference across the land/water interface ranges by about $\sim 10\%$, whereas the respective $-I_p$ differences are higher ($\sim 25\text{--}30\%$; see Figure 11), suggesting that R_{ice} cannot be considered as the exclusive contributor to the observed $-I_p$ land-ocean contrast. In addition, the R_{ice} spatial-temporal variation cannot explain the absence of $+I_p$ enhancement across the ocean/land boundary nor account for the $-I_p$ spatial variations exclusively over land. For instance, the visual comparison between Figures 2a and 10 reveals an

imperfect spatial relationship between R_{ice} and $-I_p$. The latter is exemplified by e.g., the relatively higher continental R_{ice} values over the northern U.S. High Plains (Figure 10) coinciding with the smallest $-I_p$ values across the entire CONUS (Figure 2a).

As for the $\{C_{pr}, -I_p\}$ temporal-spatial patterns, these do not exhibit any consistent behavior (finding 7 and Figures 12a–12d). For example, the temporal-spatial C_{pr} variation in region 1 mainly reveals the transition from the summer convective activity (June–August, with higher cloud tops hence lower C_{pr} ; Figures 12a and 12b) to a more stratiform precipitation regime (September to October, with lower cloud tops hence higher C_{pr} ; Figures 12a and 12b). In contrast, the $-I_p$ temporal-spatial variation (Figures 12c and 12d) is consistent across both precipitation regimes. As a result, the claims in Orville [1990], according to which the thundercloud vertical development controls the observed latitudinal $-I_p$ dependence, do not likely reflect the full story regarding the underlying physical mechanism. While this mechanism may still remain somewhat elusive and incompletely revealed in the discussions above, it is important to note that the pioneering observations made by Orville [1990] (i.e., early stages of lightning detection over the U.S.) are still partially supported by finding 3. Discussion on the possible latitudinal effects is provided next.

4.7. Additional Commentary Regarding Latitude/Longitude Averaging Effects

The implementation of the temporal-spatial I_p analysis herein allows for a closer examination of one major difference between regions 1 and 4. The findings of Figure 9a show that the $-I_p$ values exhibit a smooth monotonic transition along the continental-oceanic boundary as we move southwards in region 1. In contrast, the respective findings for region 4 (Figure 9b) indicate the absence of a similar spatial $-I_p$ gradient. Arguably, the temperature gradient across region 1 (i.e., meridional, not shown) is expected to be more prominent than region 4 (i.e., zonal, not shown), therefore enhancing the effects driven by the land-sea circulation [e.g., see Arritt, 1993; Lewandowska and Falkowska, 2013]. Although the NaCl presence in the atmosphere is fundamentally associated with the oceanic environment, the low-level sea-breeze induced circulation across the coastlines, especially during the typically warmer months, is expected to further promote the NaCl presence just inland over the adjacent continent. The same expectation is valid for the ice crystals, an argument further supported by the spatial distribution of R_{ice} (Figure 11a). Regardless of which of the postulated forcing factors is in fact controlling the $-I_p$ oceanic-continental contrast, we speculate that the temporal-spatial gradients exhibited by the $-I_p$ over region 1, and their absence over region 4, could be partially attributed to the effects induced by the land-sea circulation.

5. Conclusions

This study examined several different types of datasets to address why oceanic $-I_p$ values are typically larger than those over continents. We have provided evidence that the oceanic $-I_p$ enhancement is likely related to a real physical phenomenon, thereby not associated to retrieval artifacts, in line with Said *et al.* [2013] and Zoghzyghy *et al.* [2015]. Attachment processes concerning the $-CG$ leader propagation could play a role given the substantial differences in the respective electrical conductivities and the observed $-CG$ leader propagating speeds [Williams *et al.*, 2012; Zoghzyghy *et al.*, 2015]. However, it is still uncertain whether such processes can play a leading role, at least on the temporal-spatial scales studied herein. Given the differences between space charge generation from aqueous and land surfaces, the effect of coronae [e.g., Williams and Heckman, 1993; Chauzy and Soula, 1999] could also be partially contributing nonetheless, in light of the absence of $-I_p$ enhancement over fresh water a principal role to this mechanism cannot be granted. In addition, the $-I_p$ values are clearly independent of cloud top heights as argued in Orville [1990], although our findings partially support the latitudinal dependence found by the same author. Temporal-spatial variations in SSS cannot likely contribute to respective $-I_p$ variations, further contradicting the findings in Chronis [2012]. To fully ascertain the latter, $-I_p$ variations (or other lightning flash proxies) over pristine oceans should be compared to additional Aquarius SSS retrievals.

This study also revisited the argument according to which “on average, the oceanic $-I_p$ values are larger than the continental ones” [e.g., see Orville and Huffines, 2001; Orville *et al.*, 2011]. Our findings show that this argument requires refinement in that the oceanic $-I_p$ enhancement is most prominent (1) during the wet season and (2) when the respective averaging is meridional. In contrast, when the $-I_p$ values are zonally averaged,

despite that the $-I_p$ oceanic-continental contrast is still evident, the seasonal preference shown in region 1 is nearly absent.

Our findings support the notion that the oceanic $-I_p$ enhancement likely relates to a physical mechanism that modulates the thundercloud potential (and possibly the breakdown voltage), in partial agreement with earlier arguments made by Brook [1992, 1995] from observations of larger $-I_p$ values in winter storms. The strongest evidence in favor of this hypothesis is the gradual/blurred $-I_p$ variation across the land/ocean boundary. The latter situation has shown distinct preference over a region and during a season, where dynamical mass transfer is expected to be more pronounced. Conversely, our findings also suggest that neither NaCl or R_{ice} alone can universally explain the observed ocean/land $-I_p$ contrast. For instance, if we argued that, e.g., R_{ice} drives the contrast between oceanic and continental $-I_p$, then why not expect the same mechanism to also drive the continental $-I_p$ variation? The results indicate that this is not the case, but rather each of the proposed candidates has unique pros and cons, effectively highlighting the apparently complex nature of the problem. In the same context, if we argued that, e.g., NaCl drives the ocean/land contrast then problems arise from the highlighted seasonal $-I_p$ variation. One could further speculate that more complex mechanisms involving both variables, such as the affinity of NaCl for ice nucleation [Wise *et al.*, 2012; Wagner and Mohler, 2013], might also be important but establishing this argument would require more dedicated research. Along these lines, emphasis in future studies could be given in the explicit role of the highlighted wet season and its possible links to other cloud characteristics such as, e.g., cloud horizontal extent as an effective property for charge storage (i.e., as in electrical capacitors).

Despite that the physical mechanism in question remains elusive and more complicated than previously suggested, the findings herein are interesting on their own merits. This is because they underline the need for more in-depth exploration of flash properties other than “counts” but they also contextualize our knowledge gap in terms of the lightning’s linkages to atmospheric processes other than the systematically studied severe weather. In the context that the majority of experiments on hydrometeor electrostatic charging are based on distilled or de-ionized water, it is easily understood that the quantification of the role of soluble constituents (e.g., such as NaCl) in the thunderstorm charging processes is of critical importance for furthering our understanding of lightning and thunderstorm electrification [Jayaratne, 2003].

The upcoming Geosynchronous Lightning Mapper (GLM) [Goodman *et al.*, 2013] mission is expected to shed more light in several questions raised in this paper. For example, the GLM observational continuum of oceanic flash properties such as, e.g., flash radiances, which have also revealed larger values than the respective continental [Beirle *et al.*, 2014], might further contribute in identifying the physical mechanism responsible for this particular oceanic lightning flash superiority.

Acknowledgments

The first author acknowledges the support by Steve Goodman and the GOES-R System Program as part of the Proving Ground and Risk Reduction programs. The authors greatly appreciate the comments by Earle Williams and Ken Cummins. We also extend our thanks to Ryan Said, Ted Mansell, Walter Lyons, and George Chronis for their input. The NLDN data were kindly provided by Vaisala Inc. through a UAH/ESSC memorandum of agreement, for research purposes only. The NLDN data are available at <http://thunderstorm.vaisala.com>.

References

- Anderson, R. B., and A. J. Eriksson (1980), Lightning parameters for engineering application published in *Electra* 69.
- Arritt, R. W. (1993), Effects of the large-scale flow on characteristic features of the sea breeze, *J. Appl. Meteorol.*, *32*, 116–125.
- Avila, E. E., R. G. Pereyra, G. G. A. Varela, and G. M. Caranti (2002), The effect of the cloud-droplet spectrum on electrical charge transfer during individual ice-ice collisions, *Q. J. R. Meteorol. Soc.*, *128*, 1669.
- Beirle, S., W. Koshak, R. Blakeslee, and T. Wagner (2014), Global patterns of lightning properties derived by OTD and LIS, *Nat. Hazards Earth Syst. Sci.*, *14*, 2715–2726, doi:10.5194/nhess-14-2715-2014.
- Biagi, C. J., K. L. Cummins, K. E. Kehoe, and E. P. Krider (2007), National Lightning Detection Network (NLDN) performance in southern Arizona, Texas, and Oklahoma in 2003–2004, *J. Geophys. Res.*, *112*, D05208, doi:10.1029/2006JD007341.
- Blakeslee, R. J., D. M. Mach, M. G. Bateman, and J. C. Bailey (2014), Seasonal variations in the lightning diurnal cycle and implications for the global electric circuit, *Atmos. Res.*, *135–136*, 228–243.
- Blanchard, D. C. (1989), The size and height to which jet drops are ejected from bursting bubbles in seawater, *J. Geophys. Res.*, *94*, 10,999–11,002, doi:10.1029/JC094iC08p10999.
- Brook, M. (1992), Breakdown electric fields in winter storms, *Res. Lett. Atmos. Electr.*, *12*, 47–52.
- Brook, M. (1995), A study of lightning in winter thunderstorms and the analysis of thunderstorm over flight data, NASA Final Rep., Grant NAG-066, New Mexico Institute of Mining and Technology, 20 May.
- Changnon, S. A. (1988), Climatology of thunder events in the conterminous United States. Part I: Temporal aspects, *J. Clim.*, *1*, 389–398.
- Chauzy, S., and S. Soula (1999), Contribution of the ground corona ions to the convective charging mechanism, *Atmos. Res.*, *51*(3), 279–300, doi:10.1016/S0169-8095(99)00013-7.
- Christian, H. J., et al. (2003), Global frequency and distribution of lightning as observed from space by the Optical Transient Detector, *J. Geophys. Res.*, *108*(D1), 4005, doi:10.1029/2002JD002347.
- Chronis, T. (2012), Preliminary lightning observations over Greece, *J. Geophys. Res.*, *117*, D03113, doi:10.1029/2011JD017063.
- Chronis, T., E. Williams, and E. Anagnostou (2006), Evidence of tropical forcing of the 6.5 wave from lightning observations over Africa, *J. Atmos. Sci.*, *64*, 3717–3721.

- Chronis, T., R. Said, K. Cummins, W. Koshak, E. Williams, E. McCaul, G. Stano, and M. Grant (2015a), Climatological diurnal variation of negative CG lightning peak current over the continental United States, *J. Geophys. Res. Atmos.*, *120*, 582–589, doi:10.1002/2014JD022547.
- Chronis, T., T. Lang, W. Koshak, R. Blakeslee, H. Christian, E. McCaul, and J. Bailey (2015b), Diurnal characteristics of lightning flashes detected over the São Paulo Lightning Mapping Array, *J. Geophys. Res. Atmos.*, *120*, 11,799–11,808, doi:10.1002/2015JD023960.
- Cooray, V., and M. Becerra (2012), Attractive radii of vertical and horizontal conductors evaluated using a self consistent leader inception and propagation model—SLIM, *Atmos. Res.*, *117*, 64–70.
- Cooray, V., and V. Rakov (2011), Engineering lightning return stroke models incorporating current reflection from ground and finitely conducting ground effects, *IEEE Trans. Electromagn. Compat.*, *53*, 773–781.
- Cooray, V., R. Jayaratne, and K. L. Cummins (2014), On the peak amplitude of lightning return stroke currents striking the sea, *Atmos. Res.*, *149*, 372–376.
- Cummins, K., E. P. Krider, and M. Malone (1998), The U.S. National Detection network and applications of cloud-to-ground lightning data by electric power utilities, *IEEE Trans. Electromagn. Compat.*, *40*(4).
- Cummins, K. L., J. A. Cramer, W. A. Brooks, and E. P. Krider (2005), On the effect of land-sea and other earth surface discontinuities on LLS-inferred lightning parameters, VIII International Symposium on Lightning Protection (S/PLDA), São Paulo, Brazil.
- Cummins, K. L., and M. J. Murphy (2009), An overview of lightning locating systems: History, techniques, and data uses, with an in-depth look at the U.S. NLDN, *IEEE Trans. Electromagn. Compat.*, *51*(3), 499–518.
- Duda, D. P., et al. (2002), An interhemispheric comparison of cirrus cloud properties using MODIS and GOES, paper presented at the 11th Conference on Cloud Physics, Am. Meteorol. Soc., Ogden, Utah.
- Fuchs, B. R., S. A. Rutledge, E. C. Bruning, J. R. Pierce, J. K. Kodros, T. J. Lang, D. R. MacGorman, P. R. Krehbiel, and W. Rison (2015), Environmental controls on storm intensity and charge structure in multiple regions of the continental United States, *J. Geophys. Res. Atmos.*, *120*, 6575–6596, doi:10.1002/2015JD023271.
- Füllekrug, M., C. Price, Y. Yair, and E. R. Williams (2002), Intense oceanic lightning, *Ann. Geophys.*, *20*, 133–137, doi:10.5194/ANGE0-20-133-2002.
- Gathman, S., and E. M. Trent (1968), Space charge over the open ocean, *J. Atmos. Sci.*, *25*, 1075–1079, doi:10.1175/1520-0469(1968)025<1075:SCOTOO>2.0.CO;2.
- Goodman, S., et al. (2013), The GOES-R Geostationary Lightning Mapper (GLM), *Atmos. Res.*, *125–126*, 34–49.
- Holle, R. L. (2014), Diurnal variations of NLDN-reported cloud-to-ground lightning in the United States, *Mon. Weather Rev.*, *142*, 1037–1052.
- Huffines, G. R., and R. E. Orville (1999), Lightning ground flash density and thunderstorm duration in the continental United States: 1989–1996, *J. Appl. Meteorol.*, *38*, 10131019.
- Hutchins, M. L., R. H. Holzworth, K. S. Virts, J. M. Wallace, and S. Heckman (2013), Radiated VLF energy differences of land and oceanic lightning, *Geophys. Res. Lett.*, *40*, 2390–2394, doi:10.1002/grl.50406.
- Jayaratne, E. R., C. P. R. Saunders, and J. Hallett (1983), Laboratory studies of the charging of soft hail during ice crystal interactions, *Q. J. R. Meteorol. Soc.*, *109*, 609–630.
- Jayaratne, R. (2003), *The Lightning Flash*, edited by V. Cooray, pp. 17–44, Institution of Electrical Engineers, London.
- Junge, C. E., and R. T. Werby (1958), The concentration of chloride, sodium, potassium, calcium, and sulfate in rainwater over the United States, *J. Meteorol.*, *15*, 417–425.
- Khemani, L. T., G. A. Monin, M. S. Naik, and A. S. Murty (1981), Chloride and sodium increases in rain from salt-seeded clouds, *J. Weather Modif.*, *13*, 182–183.
- King, M. D., S. Platnick, P. Yang, G. T. Arnold, M. A. Gray, J. C. Riedi, S. A. Ackerman, and K. N. Liou (2004), Remote sensing of liquid water and ice cloud optical thickness and effective radius in the Arctic: Application of airborne multispectral MAS data, *J. Atmos. Oceanic Technol.*, *21*, 857–875.
- Koshak, W. J., K. L. Cummins, D. E. Buechler, B. Vant-Hull, R. J. Blakeslee, E. R. Williams, and H. S. Peterson (2015), Variability of CONUS lightning in 2003–12 and associated impacts, *J. Appl. Meteorol. Climatol.*, *54*(1), 15–41.
- Kucienska, B., G. B. Raga, and R. Romero-Centeno (2012), High lightning activity in maritime clouds near Mexico, *Atmos. Chem. Phys.*, *12*, 8055–8072, doi:10.5194/acp-12-8055-2012.
- Lewandowska, A. U., and L. M. Falkowska (2013), Sea salt in aerosols over the southern Baltic. Part 1. The generation and transportation of marine particles, *Oceanologia*, *55*(2), 279–298, doi:10.5697/oc.55-2.279.
- Lyons, W. A., M. Uliasz, and T. Nelson (1998a), Large peak current cloud-to-ground lightning flashes during the summer months in the contiguous United States, *Mon. Weather Rev.*, *126*, 2217–2233.
- Lyons, W. A., T. E. Nelson, E. R. Williams, J. A. Cramer, and T. R. Turner (1998b), Enhanced positive cloud-to-ground lightning in thunderstorms ingesting smoke from fires, *Science*, *282*, 77–80, doi:10.1126/science.282.5386.77.
- Mach, D. M., R. J. Blakeslee, and M. G. Bateman (2011), Global electric circuit implications of combined aircraft storm electric current measurements and satellite-based diurnal lightning statistics, *J. Geophys. Res.*, *116*, D05201, doi:10.1029/2010JD014462.
- Mallick, S., et al. (2014), Performance characteristics of the NLDN for return strokes and pulses superimposed on steady currents, based on rocket-triggered lightning data acquired in Florida in 2004–2012, *J. Geophys. Res. Atmos.*, *119*, 3825–3856.
- Meissner, T., and F. J. Wentz (2004), The complex dielectric constant of pure and sea water from microwave satellite observations, *IEEE Trans. Geosci. Remote Sens.*, *42*(9), 1838–1849.
- Menzel, P. W., R. A. Frey, H. Zhang, D. P. Wylie, C. C. Moeller, R. E. Holz, B. Maddux, B. A. Baum, K. I. Strabala, and L. E. Gumley (2008), MODIS global cloud-top pressure and amount estimation: Algorithm description and results, *J. Appl. Meteorol. Climatol.*, *47*, 1175–1198.
- Miller, J. M. (1974), A statistical evaluation of the US precipitation chemistry network, *Proc. A. E. C. Symp. Precipitation Scavenging Champaign RDA CONF-741003*, 639–659.
- Möller, D. (1990), The Na/Cl ratio in rainwater and the sea salt chloride cycle, *Tellus B*, *42*, 254–262, doi:10.1034/j.1600-0889.1990.t01-1-00004.x.
- Muir, M. S. (1977), Atmospheric electric space charge generated by the surf, *J. Atmos. Terr. Phys.*, *39*, 1341–1346.
- Nastos, P. T., I. T. Matsangouras, and T. G. Chronis (2013), Spatio-temporal analysis of lightning activity over Greece. Preliminary results derived from the recent state precision lightning network, *Atmos. Res.*, doi:10.1016/j.atmosres.2013.10.021.
- Orville, R. E. (1990), Peak-current variations of lightning return strokes as a function of latitude, *Nature*, *342*(6254), 149–151.
- Orville, R. E., and G. R. Huffines (2001), Cloud-to-ground lightning in the United States: NLDN results in the first decade, 1989–98, *Mon. Weather Rev.*, *129*, 1179–1193.
- Orville, R. E., G. R. Huffines, W. R. Burrows, and K. Cummins (2011), The North American Lightning Detection Network (NALDN): Analysis of flash data—2001–2009, *Mon. Weather Rev.*, *139*, 1305–1322, doi:10.1175/2010MWR3452.1.
- Orville, R. R., G. Huffines, J. N. Gammon, R. Zhang, B. Ely, S. Steiger, S. Phillips, S. Allen, and W. Read (2001), Enhancement of cloud-to-ground lightning over Houston, Texas, *Geophys. Res. Lett.*, *28*(13), 2597–2600, doi:10.1029/2001GL012990.

- Pinto, O., Jr., R. B. B. Gin, I. R. C. A. Pinto, O. Mendes Jr., J. H. Diniz, and A. M. Carvalho (1996), Cloud-to-ground lightning flash characteristics in southeastern Brazil for the 1992–1993 summer season, *J. Geophys. Res.*, *101*, 29,627–29,635, doi:10.1029/96JD01865.
- Platnick, S., M. D. King, S. A. Ackerman, W. P. Menzel, B. A. Baum, J. C. Riedi, and R. A. Frey (2003), The MODIS cloud products: Algorithms and examples from Terra, *Geosci. Rem. Sens. IEEE Trans.*, *41*(2), 459–473, doi:10.1109/TGRS.2002.808301.
- Rachidi, F., and R. Thottapillil (1993), Determination of lightning currents from far electromagnetic fields, *J. Geophys. Res.*, *98*, 18,315–18,321, doi:10.1029/93JD01616.
- Rachidi, F., J. L. Bermudez, M. Rubinstein, and V. A. Rakov (2004), On the estimation of lightning peak currents from measured fields using lightning location systems, *J. Electrostat.*, *60*(2–4), 121–129, doi:10.1016/j.elstat.2004.01.010.
- Rädcl, G., C. J. Stubenrauch, R. Holz, and D. L. Mitchell (2003), Retrieval of effective ice crystal size in the infrared: Sensitivity study and global measurements from TIROS-N Operational Vertical Sounder, *J. Geophys. Res.*, *108*(D9), 4281, doi:10.1029/2002JD002801.
- Rein, M. (1996), The transitional regime between coalescing and splashing drops, *J. Fluid Mech.*, *306*, 145–165.
- Reiter, R. (1994), Charges on particles of different size from bubbles of Mediterranean Sea surf and from waterfalls, *J. Geophys. Res.*, *99*(D5), 10,807–10,812, doi:10.1029/93JD03268.
- Rivas Soriano, L., F. de Pablo, and C. Tomas (2005), Ten-year study of cloud-to-ground lightning activity in the Iberian Peninsula, *J. Atmos. Sol. Terr. Phys.*, *67*, 1632–1639.
- Rosenfeld, D., R. Lahav, A. Khain, and M. Pinsky (2002), The role of sea spray in cleansing air pollution over ocean via cloud processes, *Science*, *297*, 1667–1670, doi:10.1126/science.1073869.
- Rudlosky, S. D., and H. E. Fuelberg (2010), Pre- and post-upgrade distributions of NLDN reported cloud-to-ground lightning characteristics in the contiguous United States, *Mon. Weather Rev.*, *138*, 3623–3633.
- Rudlosky, S. D., and H. E. Fuelberg (2011), Seasonal, regional, and storm-scale variability of cloud-to-ground lightning characteristics in Florida, *Mon. Weather Rev.*, *139*, 1826–1843.
- Said, R. K., U. S. Inan, and K. L. Cummins (2010), Long-range lightning geo-location using a VLF radio atmospheric waveform bank, *J. Geophys. Res.*, *115*, D23108, doi:10.1029/2010JD013863.
- Said, R. K., M. B. Cohen, and U. S. Inan (2013), Highly intense lightning over the oceans: Estimated peak currents from global GLD360 observations, *J. Geophys. Res. Atmos.*, *118*, 6905–6915, doi:10.1002/jgrd.50508.
- Saunders, C. P. R., H. Bax-Norman, C. Emersic, E. E. Avila, and N. E. Castellano (2006), Laboratory studies of the effect of cloud conditions on graupel/crystal charge transfer in thunderstorm electrification, *Q. J. R. Meteorol. Soc.*, *132*, 2653–2673.
- Sherwood, S. C., V. T. J. Phillips, and J. S. Wettlaufer (2006), Small ice crystals and the climatology of lightning, *Geophys. Res. Lett.*, *33*, L05804, doi:10.1029/2005GL025242.
- Steiger, S. M., Orville, R. E., and Huffines, G. (2002), Cloud-to-ground lightning characteristics over Houston, Texas: 1989–2000, *J. Geophys. Res.*, *107*(D11), 4117, doi:10.1029/2001JD001142.
- Takahashi, T. (1978), Riming electrification as a charge generation mechanism in thunderstorms, *J. Atmos. Sci.*, *35*, 1536–1548.
- Toland, R. B., and B. Vonnegut (1977), Measurement of maximum electric field intensities over water during thunderstorms, *J. Geophys. Res.*, *82*, 438–440, doi:10.1029/JC082i003p00438.
- Turman, B. N. (1977), Detection of lightning superbolts, *J. Geophys. Res.*, *82*(18), 2566–2568, doi:10.1029/JC082i018p02566.
- Villari, G., and J. A. Smith (2013), Spatial and temporal variation of cloud-to-ground lightning over the continental U.S. during the period 1995–2010, *Atmos. Res.*, *124*, 137–148.
- Wagner, R., and O. Mohler (2013), Heterogeneous ice nucleation ability of crystalline sodium chloride dihydrate particles, *J. Geophys. Res. Atmos.*, *118*, 4610–4622, doi:10.1002/jgrd.50325.
- Wexler, R. (1960), Efficiency of natural rain, in *Physics of Precipitation: Proceedings of the Cloud Physics Conference, Woods Hole, Massachusetts, June 3–5, 1959*, edited by H. Weickmann, pp. 158–160, AGU, Washington, D. C., doi:10.1029/GM005p0158.
- Williams, E., and S. Heckman (2011), Polarity asymmetry in lightning leader speeds: Implications for current cutoff and multiple strokes in cloud-to-ground flashes, paper presented at 3rd International Symposium on Winter Lightning, Inst. of Ind. Sci., Univ. of Tokyo, Sapporo, Japan.
- Williams, E., and S. Stanfill (2002), The physical origin of the land-ocean contrast in lightning activity, *C. R. Phys.*, *3*(10), 1277–1292, doi:10.1016/S1631-0705(02)01407-X.
- Williams, E., et al. (2012), Resolution of the sprite polarity paradox: The role of halos, *Radio Sci.*, *47*, RS2002, doi:10.1029/2011RS004794.
- Williams, E. R. (1989), The tripole structure of thunderstorms, *J. Geophys. Res.*, *94*(D11), 13,151–13,167, doi:10.1029/JD094iD11p13151.
- Williams, E. R. (2006), Problems in lightning physics—the role of polarity asymmetry, *Plasma Sources Sci. Technol.*, *15*(2), S91–S108, doi:10.1088/0963-0252/15/2/S12.
- Williams, E. R., and S. J. Heckman (1993), The local diurnal variation of cloud electrification and the global diurnal variation of negative charge on the Earth, *J. Geophys. Res.*, *98*(D3), 5221–5234, doi:10.1029/92JD02642.
- Williams, E. R., et al. (2002), Contrasting convective regimes over the Amazon: Implications for cloud electrification, *J. Geophys. Res.*, *107*(D20), 8082, doi:10.1029/2001JD000380.
- Wise, M. E., K. J. Baustian, T. Koop, M. A. Freedman, E. J. Jensen, and M. A. Tolbert (2012), Depositional ice nucleation onto crystalline-hydrated NaCl particles: A new mechanism for ice formation in the troposphere, *Atmos. Chem. Phys.*, *12*, 1121–1134.
- Yuan, T., Remer, L. A., Pickering, K. E., and Yu, H. (2011), Observational evidence of aerosol enhancement of lightning activity and convective invigoration, *Geophys. Res. Lett.*, *38*, L04701, doi:10.1029/2010GL046052.
- Zajac, B. A., and S. A. Rutledge (2001), Cloud-to-ground lightning activity in the contiguous United States from 1995 to 1999, *Mon. Weather Rev.*, *129*, 9991019.
- Zoghoghzy, F. G., M. B. Cohen, R. K. Said, N. G. Lehtinen, and U. S. Inan (2015), Ship-borne LF-VLF oceanic lightning observations and modeling, *J. Geophys. Res. Atmos.*, *120*, 10,890–10,902, doi:10.1002/2015JD023226.